OPEN ACCESS
IOP Publishing
Semiconductor Science and Technology
Semicond. Sci. Technol. **37** (2022) 013001 (29pp)
https://doi.org/10.1088/1361-6641/ac3962

Topical Review

Recent progress in red light-emitting diodes by III-nitride materials

Daisuke Iida and Kazuhiro Ohkawa*

Computer, Electrical and Mathematical Sciences and Engineering (CEMSE) Division, King Abdullah University of Science and Technology (KAUST), Thuwal 23955-6900, Saudi Arabia

E-mail: kazuhiro.ohkawa@kaust.edu.sa

Received 27 July 2021, revised 8 September 2021
Accepted for publication 12 November 2021
Published 26 November 2021

Abstract

GaN-based light-emitting devices have the potential to realize all visible emissions with the same material system. These emitters are expected to be next-generation red, green, and blue displays and illumination tools. These emitting devices have been realized with highly efficient blue and green light-emitting diodes (LEDs) and laser diodes. Extending them to longer wavelength emissions remains challenging from an efficiency perspective. In the emerging research field of micro-LED displays, III-nitride red LEDs are in high demand to establish highly efficient devices like conventional blue and green systems. In this review, we describe fundamental issues in the development of red LEDs by III-nitrides. We also focus on the key role of growth techniques such as higher temperature growth, strain engineering, nanostructures, and Eu doping. The recent progress and prospect of developing III-nitride-based red light-emitting devices will be presented.

Keywords: InGaN, metalorganic vapor-phase epitaxy, red light-emitting diodes, full width at half maximum, peak wavelength shift

(Some figures may appear in color only in the online journal)

1. Introduction

III-nitride semiconductors enable a wide spectral range from the ultraviolet to the infrared. In particular, InGaN can offer emission across the entire visible range corresponding to a bandgap energy of 0.67–3.42 eV by tuning the alloy composition [1, 2]. InGaN can emit any visible light, and it is suitable for use in white illuminations and full-color displays. In 2010, InGaN-based violet and blue light-emitting diodes (LEDs) realized an extremely high wall-plug efficiency (WPE) at 84% [3] and 81% [4], respectively. This is near the fundamental limitation of the materials.

To achieve the white emissions, blue or violet LEDs are coupled with wavelength-converting phosphors, which are the most efficient white light sources [4–7]. White LEDs have been widely spreading for lighting, which is contributed to saving tremendous energy. Currently, a topic of considerable interest is full-color displays by LEDs. Tiny LED chips on the micrometer scale (e.g. 10–100 μm squares) can adopt to all displays including ultra-high definition television, smartphones, smartwatches, virtual reality, and augmented reality. Micro-LED offers high luminance, high ambient contrast ratio, high resolution, energy savings, long lifetimes, fast response, wide view angles, lightweight system etc [8, 9]. These applications require high-performance light-emitting devices with emission in three primary colors: red, green, and blue (RGB).

* Author to whom any correspondence should be addressed.

Nitride semiconductors are superior candidates for full-color micro-LEDs. The InGaN-based light-emitting devices are attractive for the next generation of displays by micro-LED chips because the III-nitride materials can emit RGB colors by tuning the bandgap energy. However, red LEDs are made from the AlGaInP material because of their outstanding high external quantum efficiencies (EQEs) (>60%) [10]. In general, the miniaturization of LEDs can reduce the EQE due to the Shockley–Read–Hall (SRH) nonradiative recombination in the form of sidewall damage during the dry etching process [11–14]. Especially, the AlGaInP-based red micro-LEDs have been reported to suffer from a significant efficiency reduction because of the high surface recombination and long carrier lifetime [15–18]. The efficiency of LEDs strongly depends on the device dimensions, which is a fundamental issue for a unique physical property of the material—the limited efficiency of micro-LEDs based on AlGaInP materials. In contrast, InGaN-based blue micro-LEDs have demonstrated remarkable performance by reducing the device dimensions. The peak EQE was reported to be as high as 33% when the device dimensions shrank to less than $20 \times 20\ \mu m^2$ [19]. The emission peak wavelength has excellent high stability with current increases. Therefore, the performance of blue micro-LEDs has already fulfilled the feasibility of micro-LED applications. The results suggest that nitride-based micro-LEDs can realize a higher efficiency than AlGaInP when the device dimension shrinks. Therefore, interest in red micro-LED production based on III-nitride materials instead of the AlGaInP ones has grown.

There are crucial matters at longer emission wavelengths than blue. First, the luminous efficiency of green LEDs has improved over time: It was reported that the maximum EQE exceeded 50% using standard chip sizes [20–22]. However, the green LEDs typically suffer from an emission peak wavelength shift and color purity [23–25]. These phenomena are common features of InGaN-based LEDs with high In content. Normally, the peak shift behavior is attributed to the internal electric field via strain in the active region [26, 27]. The transition energy depends on the injection current due to screening of the electric field. Besides, the In fluctuation in InGaN quantum wells (QWs) will have a large influence on the full width at half maximums (FWHMs). Thus, green LEDs desire small peak wavelength shifts and narrow FWHMs to improve the color gamut in International Commission on Illumination (CIE) 1931.

In recent years, several companies have announced InGaN-based red LEDs on each platform technology. Therefore, interest in InGaN materials in red micro-LEDs has grown. Nitride-based red LEDs can lead to monolithic RGB LEDs constructed from the same material system for next-generation display applications. However, InGaN red LEDs have significantly reduced EQE when the In content increases in the InGaN active region. The low efficiency of red LEDs is the bottleneck for RGB micro-LEDs development. It has been more than 20 years since the first InGaN-based red LEDs were demonstrated by the Nichia company [28]. Currently, the EQE of InGaN-based red LEDs in the spectral range at 630 nm is as low as 3% at standard current density (e.g. >10 A cm^{-2}) [29]. The major challenge for achieving InGaN-based red LEDs is the significant reduction in the EQE due to the degradation of InGaN crystal quality. In general, the InGaN active region can obtain a longer emission wavelength with increasing In content. The In content of InGaN-based red LEDs is as much higher than 0.3 and two times that of blue LEDs. As a result of the increase in In content in the active region, the crystal quality of InGaN can be degraded by fundamental issues such as low-temperature growth [30, 31], and large lattice mismatch [32, 33]. Besides, the emission peak wavelength shift due to the internal electric field is a more serious issue than in green LEDs [29, 34–36]. The InGaN-based red LEDs are suffered with strong quantum-confined Stark effect (QCSE), resulting in more wavelength shifts and lower internal quantum efficiencies (IQEs). The highly efficient red emissions by InGaN are extremely difficult to realize for these issues.

The object of this paper is to review red LEDs based on nitride semiconductors with emission wavelengths over 600 nm. We then comprehensively explain their crystal growth technology and their characteristics. Various methods have been proposed to realize red emission from nitride semiconductors, and we will introduce several such approaches. This paper is organized as below. Section 2 introduces the fundamental problems such as InGaN growth temperature, followed by the description of approaches to improve the crystal quality of (0001) *c*-plane InGaN such as metalorganic vapor-phase epitaxy (MOVPE) simulation, growth rate, and strain relaxation. Section 3 describes the strain engineering of the (0001) *c*-plane InGaN active regions via InGaN superlattices and strain compensating. Section 4 introduces the InGaN-based LEDs with (000–1) *c*-plane, semipolar, and nonpolar. In section 5, other interesting approaches will be explained in light of the various low-dimensional structures such as quantum dots (QDs), nanowires (NWs), and platelets. In section 6, we show an alternative approach to obtain red emission: Eu-doping in nitride semiconductors. Those approaches will likely minimize the problems above. In section 7, an overview of the current device performance will be presented. We will also review the state-of-the-art performance of InGaN-based red LEDs.

2. High-quality and high-In-content InGaN prepared via raised growth temperature

The MOVPE is well known to produce blue/green light-emitting devices. However, the EQE of nitride-based light-emitting devices in the red range is remarkably low at several percent [28, 29, 35] due to the immiscibility of InN and GaN leading to the degradation of the crystal quality of InGaN at high In contents [37]. InGaN alloys are usually grown from 700 °C to 800 °C because In adatoms are easily re-evaporated during growth with increasing growth temperature [30, 38]. It is well known that InN can easily decompose at a much lower temperatures than GaN and AlN based on the relationship between equilibrium pressure and growth temperature for group III-nitride semiconductors [39]. Thus, high-In-content InGaN is fundamentally difficult to grow with high crystal

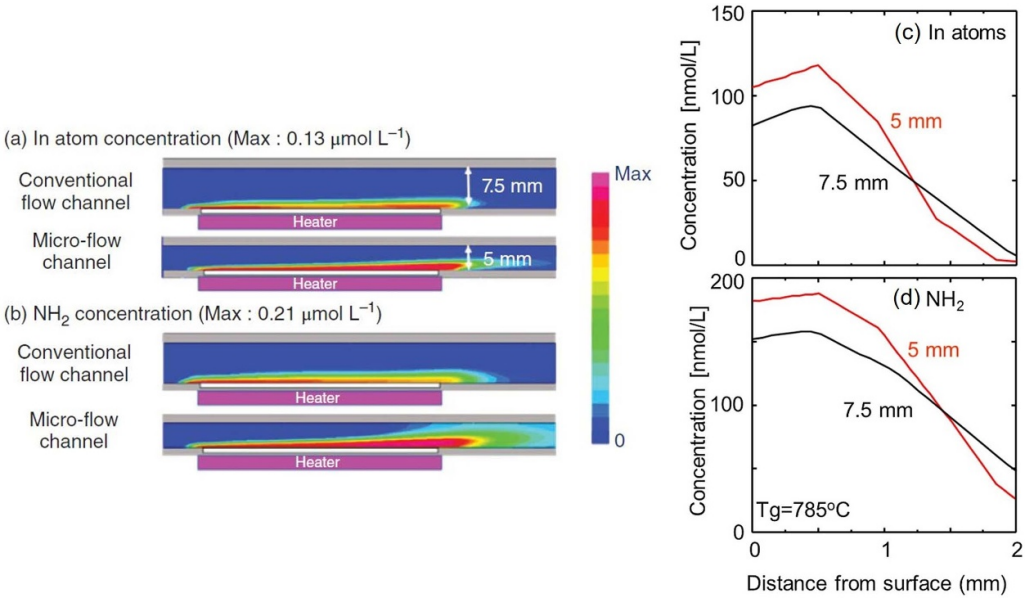

Figure 1. Concentration distributions of (a) In atoms decomposed from TMIn. [50] John Wiley & Sons. Copyright © 2020 Wiley-VCH Verlag GmbH & Co. KGaA. All rights reserved; and (b) NH_2 molecules from NH_3 in conventional and micro-flow channels. The amount of precursors are identical in both flow channels. Reproduced from [38]. CC BY 4.0. Simulated distributions of (c) In atoms and (d) decomposed NH_2 concentrations around the substrate surface at the wafer center. The red and black lines are in cases of the micro-flow channel (5 mm height) or conventional flow channel (7.5 mm height), respectively. The flow amounts of each precursor are the same in both cases.

quality because one of the crucial factors for controlling the crystallinity is by growth temperature. (0001) *c*-plane InGaN growth at low temperatures has some issues such as phase separation [40, 41], rough surfaces [42, 43], and high impurities [44, 45]. Thus, higher growth temperatures are essential to growing high-quality InGaN active regions. In this section, we present growth techniques to improve the crystal quality of conventional (0001) *c*-plane InGaN.

2.1. Simulation and experiments by MOVPE

III-nitride semiconductor crystal growth by MOVPE complicates the growth process versus the other materials such as phosphides and arsenides [46–48]. Those growth conditions have been optimized by many experiments. Numerical calculations are also helpful to understand the feasibility of material growth by MOVPE system. The results require comparison with experiments to validate computational approaches. Theoretical works have been carried out to investigate the growth of In(Ga)N [30, 38, 49–52]. Such analysis has contributed to the understanding of In(Ga)N growth in tandem with experimental results. The computational approaches are crucial for understanding the complicated phenomena of crystal growth.

Regarding the thermodynamic calculations, raised-pressure MOVPE was proposed to overcome the stability of In(Ga)N growth at a high temperature [53–55]. In experiments, high-In-content InGaN (as high as 0.42) was demonstrated by 800 °C growth temperature at 200 kPa [55]. The peak emission wavelength was presented at the deep red emission range up to 720 nm. The crystal quality of InN drastically improved by high temperature growth at up to 865 °C at 2 MPa [54]. High-pressure growth provides the material with thermal stability under thermodynamic equilibrium states.

Also, the growth of III-nitrides materials has been numerically investigated by computational fluid dynamics (CFD) simulation [38, 50]. These CFD simulations are based on a huge number of chemical reactions, which agrees well with the experiment results both qualitatively and quantitatively. Crystal growth modeling can provide useful information related to the optimal growth conditions and reactor designs.

We previously reported the modification of the inside flow channel's height from 7.5 to 5.0 mm by following the InGaN MOVPE CFD simulation [38, 50, 56]. This is the so-called 'micro-flow channel technique'. This technique helped develop yellow to red LEDs. Figure 1 shows the modeling of In atoms and NH_2 molecules in both flow channels by the simulation [38, 50]. The numerical simulation results found that the concentration of the In atoms and NH_2 molecules in the vicinity of the growth surfaces were improved by 27% and 20% using the 5 mm height flow channel versus a conventional flow channel, respectively. The decomposition efficiency of the precursors improved, which leads to grow of high In-content InGaN. When the micro-flow channel technique was used, the 600 nm emission wavelength LEDs can produce a growth temperature that is 60 °C higher than the conventional flow channel [56]. The IQE of 600 nm emission wavelength LEDs was improved from 4% to 18% using the thinner flow channel. The higher growth temperature improved the high-In-content InGaN crystal quality. Also, the deep red emission at 740 nm was first demonstrated due to the In pulling effect by strain relaxation when the number of the QWs increased from 5 to 16 [56]. Clearly, this micro-flow channel technique is a

very effective method for producing long emission wavelength devices by InGaN.

MOVPE reactors should become larger with scale-up of wafer diameters (e.g. 8 inches); concurrently, material consumption during production has grown. This is a huge cost for each growth. Growth modeling indicates some crucial information prior to growing the devices, which will save time and costs. In the future, computational methods can facilitate optimal growth modeling leading to high quality crystals and devices.

2.2. Growth rate

The growth rate of InGaN is an essential factor for improving crystalline quality. This parameter is significantly related to various aspects of the growth phenomena such as crystalline defects, impurities, and surface flatness. In general, the lower growth rate in the active region is preferred to obtain good crystallinity. The low growth rate can be obtained via a high V/III ratio, which can compensate for NH_3 clacking efficiency at a low growth temperature. The lower growth rate can minimize the formation of point defects, In-rich clustering, In droplets, and impurity incorporations in the InGaN active region due to enhanced surface migration of adatoms. The InGaN layers can enhance step-flow growth and can lead to a smooth surface with sharp interfaces in the QW structures. These efforts have improved the device performance. However, InGaN red QWs are not reasonable to use at a low growth rate due to the significantly high In re-evaporation during InGaN growth even if a high V/III ratio is achieved. This is a complicated issue for high-In-content InGaN QW growth.

Importantly, a higher growth rate has also been proposed to optimize the InGaN growth for red emission [57]. This approach is the complete opposite of typical blue InGaN QWs growth condition, but the crystal quality of InGaN red QWs was improved. These data suggest that the incremental growth rate enhances the In incorporation rate into InGaN because of the In re-evaporation reduction. Figure 2 shows that the In content in InGaN is dependent on growth rates (0.5–5.2 nm min^{-1}) and growth temperatures [57]. The surface defect density reduction and the smooth surface on the InGaN QW were realized due to improved surface migration of adatoms with increased growth temperatures. The bright luminous area in InGaN QWs by photoluminescence (PL) measurements was expanded using optimal high growth rate conditions. Alhassan *et al* also reported the highly efficient green LEDs using the high growth rate (6 nm min^{-1}) for InGaN QWs [58]. Therefore, a high growth rate of high-In-content InGaN QWs is effective to improve the crystal quality. However, it considers that the point defects and impurities may increase with a higher growth rate because the V/III ratio decrease (i.e. III-material precursors increase). Also, according to thermodynamics, the low V/III ratio is not favorable to grow high-In-content InGaN [30]. The optimization of the increased growth rate is a crucial factor underlying high-In-content InGaN at high temperatures.

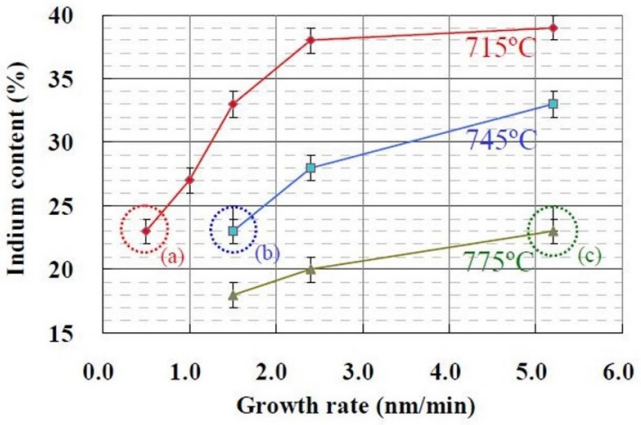

Figure 2. Indium content dependence on growth conditions. [57] John Wiley & Sons. Copyright © 2013 WILEY-VCH Verlag GmbH & Co. KGaA, Weinheim.

2.3. Relaxed InGaN underlying layers

The proper In content in the strain-relaxed InGaN underlying layers are required to produce highly efficient light-emitting devices for red emission. However, the lattice mismatch between GaN and InN is as large as 11%, which leads to the degradation of InGaN alloys by strain relaxation [33]. The crystal quality of the InGaN active region strongly depends on the in-plane lattice constant in the underlying layers. In general, the accumulation of high compressive stress in InGaN layers grown on GaN generates misfit and threading dislocations, stacking faults, trench defects, In segregation, and V-shaped pits when the stress-energy releases [33, 59–62]. The increase in defect densities depends on the In content in InGaN layers due to the lattice mismatch with GaN underlying layers. Therefore, higher In content InGaN alloys have suffered significantly from defect generation. This is a major issue in the production of InGaN devices with high In content. To solve the issue, the community needs to explore the outstanding growth technique to reduce the lattice mismatch between underlying layers and InGaN QWs. The In incorporation rate increases when the InGaN thickness increases—this is strongly involved in the in-plane stress releases during growth. A common phenomenon is the so-called 'compositional pulling effect', which is attributed to an increase in the *a*-lattice constant [32, 63, 64].

These phenomena lead to the concept of InGaN pseudo-substrates which have less lattice mismatch with the epitaxial structures composed of InGaN to fabricate high-performance LEDs in the red spectral range. Previously, a high degree of relaxation of InGaN underlying layers provided the improved emission efficiency of InGaN active layers in the green spectral range, which represented a proof-of-concept for strain-relaxed InGaN [65, 66]. In recent years, the strain-relaxed InGaN layers aim to further increase the *a*-lattice constant to obtain equivalent strain in the red QWs as the blue QWs grown on typical GaN layers. Various efforts have been developed to produce high-quality strain-relaxed InGaN layers. The goal is

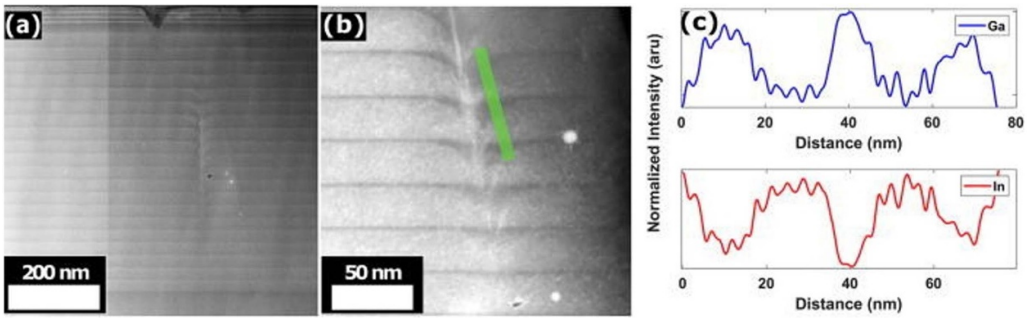

Figure 3. (a) HAADF-STEM of sample 8% SB, showing a consistent flat growth of InGaN layers. (b) HAADF-STEM of a dislocation showing back-filling of the generated V-pits. (c) EDS along the line profile in (b) showing the backfill of the V-pits demonstrates an increase in the Ga content with a decrease in In. Reprinted from [68], with the permission of AIP Publishing.

to obtain large in-plane *a*-lattice constants via strain relaxation of InGaN layers with superior benefits to minimize the lattice mismatch with InGaN QWs for red emission and suppress the generation of misfit dislocations. Furthermore, the reduction in lattice mismatch can lead to an increase in InGaN growth temperature due to the compositional pulling effect, which can also improve the crystallinity of InGaN QWs. The low in-plane strain in InGaN QWs also leads to a reduction in QCSE to ultimately improve IQE. These approaches are a very important technology for the development of highly efficient InGaN red LEDs. Here, we review several techniques for fabricating strain-relaxed InGaN pseudo-substrates.

2.3.1. Periodic InGaN structures. In general, strain relaxed InGaN layers grown on GaN layers suffer from rough surfaces and defects [63, 67]. A periodic InGaN/GaN structure (semi-bulk InGaN layers) enlarge the in-plane lattice parameter. Pantzas *et al* reported that an $In_{0.09}Ga_{0.91}N$ layer was relaxed to a degree of 0.15 by MOVPE [67]. Similarly, Eldred *et al* demonstrated a highly relaxed semi-bulk InGaN as shown in figure 3 [68]. Figure 3(a) shows the high-angle annular dark-field scanning transmission electron microscopy (HAADF-STEM) image of the semi-bulk $In_{0.08}Ga_{0.92}N$ capped with three-period InGaN QWs. The semi-bulk structure was obtained and had consistent and flat growth for the InGaN/GaN layers across 20 periods. The V-pit was back-filled with GaN interlayers as shown in figures 3(b) and (c). This InGaN achieved a high degree of relaxation of ∼0.7. The same group obtained semi-bulk InGaN with In contents of 6%, 7.8%, 9%, and 10.2%. This corresponded to degrees of relaxation of 0.55, 0.75, 0.8, and 0.85, respectively. This approach maintains smooth surfaces and is acceptable for further epitaxial growth. Semi-bulk structures are favorable for producing high-quality InGaN templates. The authors demonstrated that the InGaN QWs grown on those InGaN templates had a large redshift of 12–35 nm.

Däubler *et al* demonstrated metamorphic InGaN buffer layers (i.e. linear composition-graded InGaN with GaN interlayers). This material had an enlarged *a*-lattice constant by plasma-assisted molecular beam epitaxy [69]. Metamorphic InGaN templates provided 45 °C higher growth temperature for InGaN QWs versus the same QW structures grown on conventional GaN templates due to a pronounced compositional pulling effect. Furthermore, the QWs grown on the metamorphic InGaN templates obtained two-fold more IQE enhancement by improved crystallinity and lower QCSE. The metamorphic InGaN technique led to red emission QWs at 640 nm with comparable IQE (20%–30%) for green emission QWs.

2.3.2. InGaN on porous GaN. Strain-relaxed InGaN layers on top of porous GaN were demonstrated by Pasayat *et al* [70, 71]. The benefit of porous GaN is a reduction in the mechanical stiffness of the crystal. This feature allows strain relaxation of pre-strained InGaN prior to GaN porosification. This shows that the degree of relaxation of InGaN layers can be tuned via the volumetric porosity of the GaN layers. However, these InGaN pseudo-substrates presented surface defects with a degraded surface morphology. The same group also improved the crystal quality of InGaN pseudo-substrates using V-defect-free GaN layers on porous GaN pseudo-substrates [72]. The 100 nm thick InGaN layer with an In content of 0.12 offers 65% strain relaxation with a smooth surface morphology (figures 4(a) and (b)). The *a*-lattice constant was as large as 3.216 Å (figure 4(a)) and corresponded to fully relaxed InGaN with an In content of 0.076. The strain relaxation behavior has markedly thicker InGaN layers. The relaxation increases with thickness. The InGaN layers were not influenced by the GaN capping layer thicknesses (figure 4(a)). However, in the case of no GaN porous structures, the 200 nm thick InGaN layer was strained on the typical GaN layer of a sapphire substrate (figure 4(c)). This novel InGaN pseudo-substrate technology is highly versatile, and it can be used not only for InGaN but also for AlGaN and conventional substrates (e.g. sapphire, Si, SiC, etc) [73].

The 632 nm wavelength InGaN red micro-LEDs were demonstrated grown on InGaN pseudo-substrates using GaN on porous GaN technique [74]. LEDs composed of the strain-relaxed $In_{0.04}Ga_{0.96}N$ layer with a relaxation degree of 0.56 had a peak emission at 632 nm of 10 A cm^{-2}. This was an on-wafer EQE of 0.2%. The devices achieved a large redshift value of 56 nm at 5 A cm^{-2} attributed to the strain reduction by the porous underlying layers. Other LED performances on

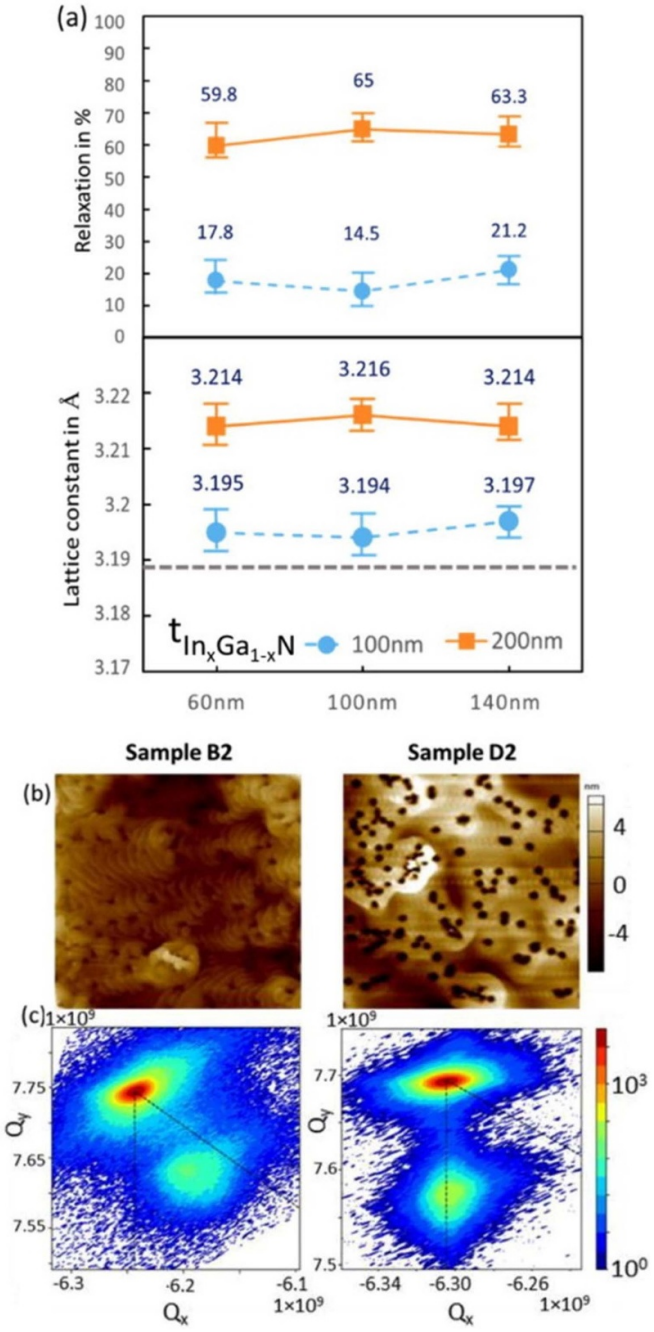

Figure 4. (a) Relaxation and a-lattice constant of 100 nm (circle) and 200 nm (squares) thick $In_xGa_{1-x}N$ layers grown on GaN-on-porous-GaN pseudo-substrates with different GaN cap layer thicknesses. The dotted gray straight line in the bottom figure corresponds to the lattice constant of the coherently strained $In_xGa_{1-x}N$ layer grown on the co-loaded GaN on a sapphire reference sample. (b) The 5 μm × 5 μm atomic force microscopy images of sample B2 (GaN cap thickness = 100 nm, $In_xGa_{1-x}N$ thickness = 200 nm) on the left and sample D2 ($In_xGa_{1-x}N$ thickness = 200 nm grown strained on a co-loaded GaN-on-sapphire wafer) on the right. (c) Reciprocal space maps of samples B2 (left) and D2 (right) around the GaN (−1–124) reflection. Reprinted from [72], with the permission of AIP Publishing.

similar InGaN pseudo-substrates were reported with redshift values of 40 and 45 nm at green emission ranges [70, 72]. The enhancement of In content incorporation into InGaN QWs was attributed to the compositional pulling effect by a-lattice constant increases.

2.3.3. Novel InGaN pseudo-substrate. Soitec developed a novel InGaN pseudo-substrate (InGaNOS substrate) based on Smart Cut^{TM} and epilayer transfer technologies [75–79]. This substrate is composed of a thin and relaxed InGaN seed layer (800 × 800 μm^2 or 500 × 500 μm^2) on a carrier sapphire substrate with a buried oxide layer. The InGaNOS achieved a 4 inch wafer scale on a carrier sapphire substrate. InGaNOS technique provides for a reduction in the lattice mismatch between InGaN QWs and the buffer layers.

In 2017, Even *et al* reported the performance of InGaN QWs grown on the 150 nm thick relaxed InGaN buffer layers with different a-lattice constants: 3.190, 3.200, and 3.205 Å [75]. Figure 5 shows the PL spectra of InGaN multiple quantum wells (MQWs) grown on those InGaNOS substrates and typical GaN templates [75]. The peak emission of MQWs had a redshift value of 49 and 62 nm for InGaNOS-3.205 Å samples due to the compositional pulling effect. The PL intensity at 594 nm emission of the InGaNOS-3.205 Å sample was enhanced two-fold compared to that of InGaNOS-3.200 Å sample. Very recently, InGaN QWs (λ = 624 nm) grown on the InGaNOS-3.205 Å substrate with InGaN/GaN superlattices had improved material quality with a large redshift of 85 nm compared to the QWs (λ = 539 nm) grown on the GaN template [79]. This technique has crucial benefits including a high In incorporation rate as well as mitigation of the internal piezoelectric field [76].

InGaN-based red micro-LEDs (50 × 50 μm^2) were demonstrated using an InGaNOS substrate with an a-lattice constant of 3.2069 Å [77]. The dislocation density presents 2 × 10^8 cm^2 which is the same as the initial InGaN/GaN layers before the InGaNOS substrate process. The micro-LEDs achieved red emission corresponding to the narrow FWHM of 48 nm at 630 nm. The maximum EQE of 0.09% was obtained for an emission wavelength of 616 nm at 40 A cm^{-2}. However, the lattice parameter of InGaNOS substrates was still not sufficient because the additional dislocation was introduced from the QWs. The IQE value was 6.5% at 624 nm via a PL intensity ratio of LT/RT. Larger a-lattice constants can mitigate the strain leading to highly efficient InGaN red LEDs.

2.3.4. Lattice-matched substrates. The lattice-matched substrates have been proposed to fabricate high-In-content InGaN-based LEDs. There are two candidates (ZnO and $ScAlMgO_4$) that can be lattice-matched under certain InGaN layers.

According to the literature, InGaN layers were grown on ZnO substrates by pulsed laser deposition [80–82] or pulsed sputter deposition (PSD) [83]. However, the (In)GaN layers must be grown at lower temperatures (<550 °C) [84] to suppress the poor-quality interfacial Ga_2ZnO_4 and Ga_2O_3 layers [85–87]. This low-temperature growth is unsuitable for MOVPE with a major nitride epitaxial growth method. InGaN epi-layers incorporated Zn and O with high impurity levels at >10^{20} cm^{-3} from the substrates [88]. These impurities were

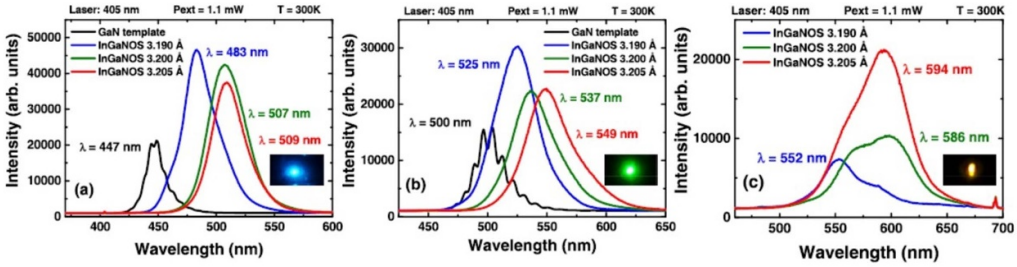

Figure 5. PL spectra at 300 K of InGaN 5QWs on InGaNOS: (a) standard blue InGaN QWs, (b) the growth temperature was decreased by 20 °C from standard blue condition, and (c) the growth temperature was decreased by 20 °C from the standard blue condition with a three times higher InGaN growth rate (the blue curve is related to InGaNOS 3.190 Å, green curve is 3.200 Å, red curve is 3.205 Å, and black curve is the reference sample.). Insets: pictures of emission under laser excitation from InGaNOS samples of (a) 3.190 Å blue luminescence, (b) 3.200 Å green luminescence, and (c) 3.205 Å amber luminescence. Reprinted from [75], with the permission of AIP Publishing.

due to the self-decomposition of ZnO by high temperature suggesting low emission efficiency of InGaN-based LEDs on a ZnO substrate [87, 89].

$ScAlMgO_4$ with the 3.249 Å *a*-lattice constant leads to a sample lattice-matched with $In_{0.17}Ga_{0.83}N$ and 1.8% lattice-mismatched with GaN. Using MOVPE growth, InGaN-based blue LEDs on (0001) $ScAlMgO_4$ substrates were demonstrated [90, 91]. GaN layers can be obtained with high crystal quality, which is comparable with GaN on sapphire [90, 92]. This implies no interfacial reaction between GaN and $ScAlMgO_4$ at high temperatures. These blue LEDs on $ScAlMgO_4$ substrates achieved a high performance similar to those on a typical sapphire substrate. Also, $In_xGa_{1-x}N/In_yGa_{1-y}N$ red MQWs ($x > 0.2$, $y \sim 0.17$) structures grown on lattice-matched $In_yGa_{1-y}N$ layers on $ScAlMgO_4$ substrates were demonstrated by Ozaki *et al* in 2019 [93]. The emission peak wavelengths were at 680 nm for the InGaN QWs grown on $ScAlMgO_4$ and 550 nm for that on sapphire at 731 °C. InGaN MQWs grown on $ScAlMgO_4$ achieved a 30 °C–40 °C higher growth temperature compared to MQWs on sapphire. This suggests a large redshift attributed to the compositional pulling effect. We also note that $ScAlMgO_4$ substrates lead to the longer emission peak wavelength of InGaN QWs due to the lower thermal conductivity (6.2 W m^{-1} K^{-1}) [94]. The critical thickness of high-In-content InGaN leads to an increase when the unstrained $In_{0.17}Ga_{0.83}N$ layers are utilized. We also expect to reduce the piezoelectric field caused by strain reduction.

Figure 6 shows the temperature dependences of the integrated PL intensities of the InGaN QWs on both $ScAlMgO_4$ and sapphire substrates at ∼625 nm emission [93]. The PL intensity ratios between LT and RT were obtained at 13.6% for the InGaN QWs on $ScAlMgO_4$ and 0.35% for that on sapphire, which indicates a large IQE enhancement factor of ∼40. In general, the *c*-plane InGaN QWs should have a blueshift with increasing excitation intensity due to the state-filling effect and the screening of the polarization field [26, 28]. In contrast, the blueshift behavior of the InGaN QWs on $ScAlMgO_4$ is noted where the peak wavelength is almost independent of the excitation intensity increase. This is the appropriate feature for fabricating display applications via micro-LEDs.

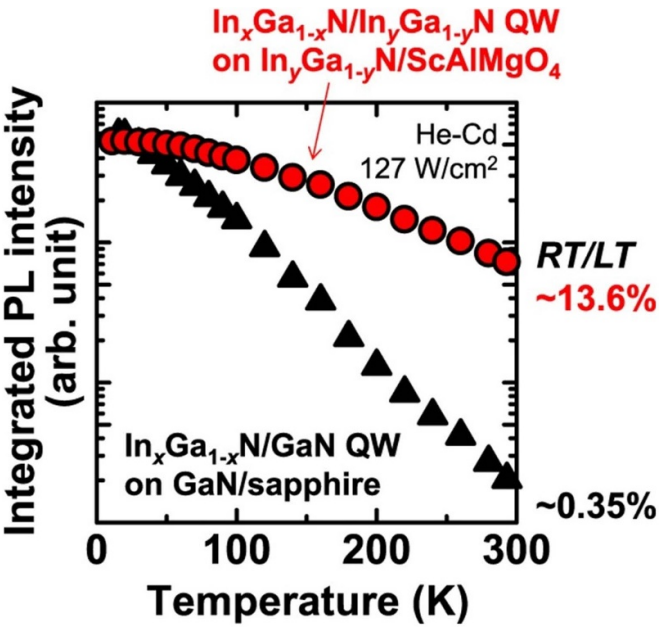

Figure 6. (a) Temperature dependence of the integrated PL intensities of the $In_xGa_{1-x}N/In_yGa_{1-y}N$ QW on $ScAlMgO_4$ and $In_xGa_{1-x}N$/GaN QW on sapphire emitting at ∼625 nm. Reproduced from [93].

2.3.5. Redshift. The redshift values of the peak emission from InGaN QWs depends on the *a*-lattice constant as listed in table 1. The redshift was obtained from the difference in peak emission wavelengths of InGaN QWs grown on InGaN and GaN templates. Some of the results suggest that the *a*-lattice constant of InGaN layers was determined by the degree of relaxation and the presumed GaN *a*-lattice constant (i.e. 3.184 Å [75]). Figure 7 shows that the redshift can be enhanced with the *a*-lattice constant as the number of InGaN layers increases suggesting the compositional pulling effect. Note that again, $ScAlMgO_4$ thermal conductivity is as low as 6.2 W m^{-1} K^{-1} [95] compared with a sapphire substrate (25 W m^{-1} K^{-1} [94]), which could affect growth temperature. InGaN QWs with a high In content have green to red spectral range emissions that were particularly more redshifted.

Table 1. Characteristics of InGaN QWs emission using InGaN templates with various In contents and relaxation degrees. The peak wavelengths were given by PL or electroluminescence (EL) measurements. The redshift values were obtained from the difference of InGaN QWs' peak wavelengths between samples grown on InGaN and GaN templates. Some of InGaN *a*-lattice constants were estimated using the reference GaN lattice constant of 3.184 Å* [75].

Affiliation	Growth method	Structure of InGaN template	In content in InGaN template	Degree of relaxation	*a*-lattice constant (Å)	MQWs λ_{peak} (nm)	Redshift (nm)	Year	Reference
Georgia Institute of Technology	MOVPE	Semibulk InGaN	0.05	0.15	3.187*	454 (PL)	17	2017	[96]
North Carolina State Univ.	MOVPE	Semibulk InGaN	0.06	0.55	3.195*	483 (PL)	12	2021	[97]
North Carolina State Univ.	MOVPE	Semibulk InGaN	0.078	0.75	3.204*	475 (PL)	31	2021	[97]
North Carolina State Univ.	MOVPE	Semibulk InGaN	0.09	0.80	3.209*	486 (PL)	35	2021	[97]
North Carolina State Univ.	MOVPE	Semibulk InGaN	0.102	0.85	3.214*	489 (PL)	43	2021	[97]
UCSB	MOVPE	InGaN/porous GaN	0.08	0.50	3.198*	527 (PL)	46	2019	[70]
UCSB	MOVPE	InGaN/porous GaN	0.118	0.65	3.216	547 (EL)	40	2020	[72]
UCSB	MOVPE	InGaN/porous GaN	0.04	0.56	3.192*	646 (EL)	56	2021	[74]
Univ. Grenoble Alpes, Soitec	MOVPE	InGaNOS	0.015	—	3.190	483 (PL)	36	2017	[75]
Univ. Grenoble Alpes, Soitec	MOVPE	InGaNOS	0.055	—	3.200	507 (PL)	60	2017	[75]
Univ. Grenoble Alpes, Soitec	MOVPE	InGaNOS	0.077	0.7	3.205	509 (PL)	62	2017	[75]
Univ. Grenoble Alpes, Soitec	MOVPE	InGaNOS	0.015	—	3.190	525 (PL)	25	2017	[75]
Univ. Grenoble Alpes, Soitec	MOVPE	InGaNOS	0.055	—	3.200	537 (PL)	37	2017	[75]
Univ. Grenoble Alpes, Soitec	MOVPE	InGaNOS	0.077	0.7	3.205	549 (PL)	49	2017	[75]
Univ. Grenoble Alpes, Soitec	MOVPE	InGaNOS	0.077	0.7	3.205	624 (PL)	85	2021	[79]
Kyoto Univ.	MOVPE	InGaN/$ScAlMgO_4$	0.17	1	3.249	680 (PL)	130	2019	[93]

We conclude that highly efficient InGaN-based pure red LEDs require the fabrication of high-quality strain-relaxed InGaN templates. The large redshift expressed the availability of increasing InGaN growth temperature, which leads to a further improvement in the crystal quality of InGaN. The benefit is not only the redshift of peak emission but also the reduction of QCSE. Due to these effects, the concept of an enlarged *a*-lattice constant for the underlying layers is expected to improve the IQE of InGaN red QWs.

2.4. GaN underlying layers

Epitaxial layers with residual strain have been introduced by the mismatches of lattice parameters and thermal expansions [98]. Thus, the residual strain is determined by substrate materials. The most common substrate is sapphire and is used for commercial blue and green LEDs. To reduce mass-production costs, several institutes and companies have developed GaN on Si technology. We show the behavior of GaN layers on several substrates for red LEDs.

InGaN-based red LEDs grown on sapphire substrates have been developed by several research groups. In general, the *a*-lattice constant of GaN layers corresponds to the residual strain. GaN layers on sapphire have a compressive strain at RT, which can be reduced as the thickness increases [98–100]. That means that the *a*-lattice constant can be increased to near the freestanding lattice constant. Our group reported the redshifting behavior of the 633 nm wavelength InGaN-based red LEDs by varying the thickness of the underlying GaN layers as shown in figure 8 [35]. The redshift was approximately 16 nm and was because the underlying *n*-GaN layer thickness increased from 2 to 8 μm. It was equivalent to a 5 °C growth temperature difference. The EL intensity of red LEDs grown on 8 μm thick *n*-GaN layers was enhanced 1.3 times relative to 4 μm thick *n*-GaN, which is attributed to the increased growth temperature of the InGaN QWs by the

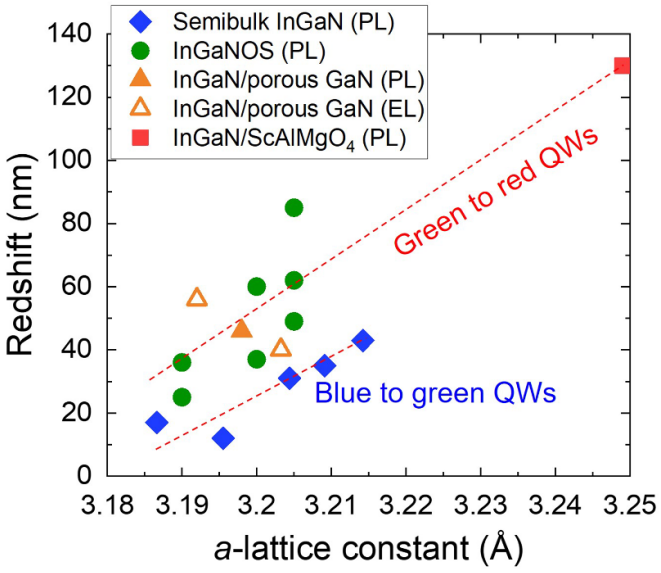

Figure 7. Redshift values of EL and PL peak wavelengths as a function of a-lattice constant of InGaN templates. The dashed lines are a guide for the eye.

a-lattice constant increases. The red LEDs have a 8 μm thick underlying n-GaN layers and offered a light-output power of 0.64 mW and an EQE of 1.6% at 20 mA (3.3 V).

To mitigate the residual strain in GaN layers, we demonstrated 665 nm wavelength InGaN-based red LEDs grown on very low strained GaN on (-201) β-Ga_2O_3 substrates in 2020 [34]. The substrates provide a low lattice mismatch ($\sim$4.7%) with GaN, which can be due to high-quality GaN layers with $\sim$1.9 ($\pm$0.2) $\times$ 10^8 cm^{-2} dislocation density [101]. The in-plane strain of GaN layers presented a very slight tensile strain by Raman analysis. The $E2$(high) peak was at 567.93 cm^{-1}, which was slightly shifted –0.07 cm^{-1} from freestanding GaN (568 cm^{-1}) [101]. In our experiments, the InGaN QWs grown on (-201) β-Ga_2O_3 substrates can increase the growth temperature by 10 °C compared to that grown on sapphire substrates. Therefore, GaN on (-201) β-Ga_2O_3 substrates can provide a great In incorporation rate into InGaN QWs leading to pure red emission.

The concept of GaN on Si technology is done at the large wafer-scale and introduces tensile strain in a GaN layer during growth. The tensile strain introduces an increase in the a-lattice constant which is enhanced during In incorporation into InGaN QWs. Note that the strain in GaN layers depends on the overall structures. Recently, highly efficient green to red InGaN-based LEDs were demonstrated by Nanchang University [20, 36, 102–104]. The tensile strain leads to a higher growth temperature at 20 °C for InGaN QWs on Si compared to that of structures on sapphire [105]. Higher growth temperatures improve the crystal quality of the InGaN QWs.

3. InGaN active regions

The device performance is fundamentally determined by the material quality. To improve the IQE of the InGaN red LEDs,

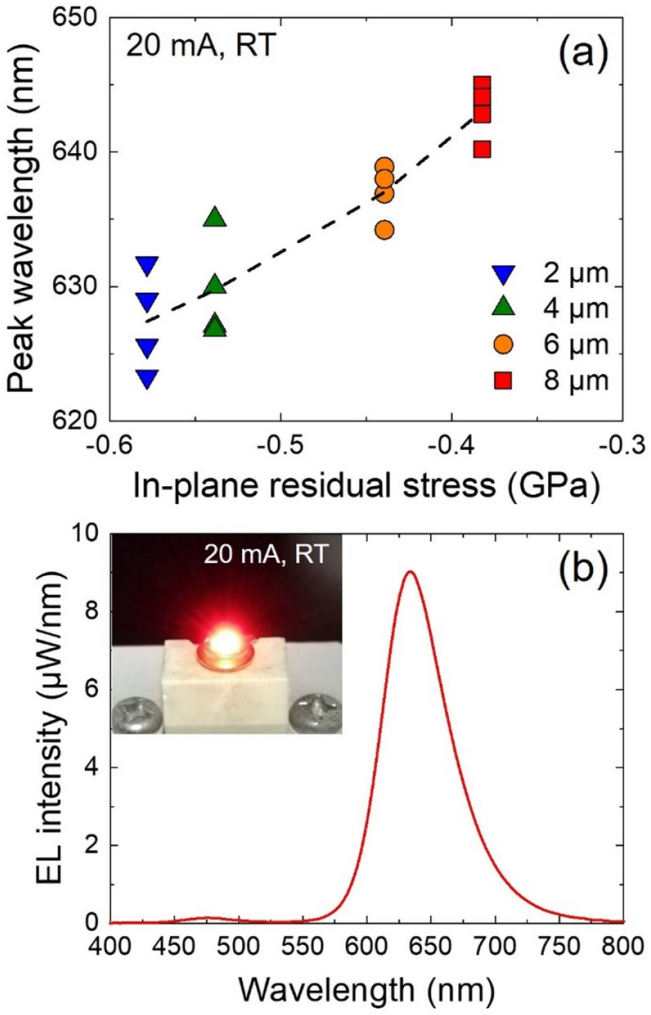

Figure 8. (a) EL peak emission wavelength as a function of in-plane stress in underlying n-GaN layers at 20 mA injection. There were four samples from each wafer. The dashed lines are visual guides for the average values. (b) EL spectrum of InGaN-based red LEDs at 20 mA. The inset shows the red LED at a 20 mA driving current. Reproduced from [35]. CC BY 4.0.

the key factors are not only the InGaN growth temperature but also the structure of its active region. The InGaN preparation layers and strain-compensating structures are promising to suppress the defects in the InGaN QWs. Thus, the structural design of the active region is a key point to improve the crystalline quality of materials. Here, we will discuss the structure of the conventional (0001) c-plane InGaN active regions toward highly efficient red emission.

3.1. Preparation layers

InGaN preparation layers are commonly used to improve the efficiency of InGaN-based blue/green LEDs. The InGaN preparation layers such as SLs can prevent the point defect propagation and slightly release of the InGaN QWs strain. Typical growth for the InGaN-based LEDs occurs during growth interruption to accommodate a drastic change in the growth condition such as from n-layers to the MQW structure.

We suggest that the growth interruption is a trigger to form point defects. Haller *et al* found that InGaN and InAlN inserting layers prevented the propagation of point defects from the underlying GaN layers [106, 107]. Also, Akasaka *et al* reported that the InGaN underlying layer reduced the nonradiative recombination centers of the QWs [108, 109]. The role of the In-incorporated material such as InGaN preparation layers reduces the defects of nonradiative recombination centers prior to growing the active region. This prevents propagation of defects into the QWs. Therefore, this technique is essential to fabricating highly efficient visible LEDs.

Meanwhile, the InGaN/GaN SLs structure is very helpful in reducing the strain in the QWs. The strain relaxation degree is not large but even slight strain relaxation is effective to improve the crystal quality of InGaN QWs and reduce the QCSE. This is the same concept as the strain relaxed InGaN templates. Meanwhile, the V-pits formed from InGaN/GaN SLs exhibited noteworthy effects while improving the overall device performance.

Hangleiter *et al* reported the mechanism underlying the unexpectedly high emission efficiency of InGaN-based QWs with V-pits [110]. The V-pit structure is induced from threading dislocations and can prevent the carrier from nonradiative recombination due to the self-screening effect [102, 111–114]. Li *et al* reported a three-dimensional numerical analysis about the role of the V-pits [115]. This model explained not only the V-pit self-screening effect but also hole injection into QWs, which proposed three-dimensional hole injection passing from *p*-GaN to QWs via V-pit structures. InGaN LEDs with green to red emissions suffer from the high forward voltage due to a high polarization field and a high potential barrier in the QWs compared to the typical blue LEDs. V-pit structures can enhance the hole injection into MQWs via the sidewalls rather than via standard *c*-plane direction due to the lower polarization charge densities in the sidewall structure of {10–11} semipolar facet planes with low In contents and thin layer thicknesses [20, 36, 102, 114, 116]. Therefore, V-pits are effective at reducing the forward voltage. The additional presence of the hole injection enhancement is also helpful to improve the efficiency limitations of LEDs. Very recently, Nanchang University's group reported highly efficient orange-red LEDs (1×1 mm^2 chip size) that included a WPE up to 24.0% at 0.8 A cm^{-2} with a wavelength of 608 nm using V-pit effects [36]. This work realized a low forward voltage operation at ∼2 V. These interesting concepts about V-pit effects can remarkably improve the WPE of the LEDs even though high dislocation densities.

We reported a hybrid MQW LED inserted a blue-green single QW underneath a main orange-red QWs [117]. This structure had improved crystal quality with orange-red QWs ($\lambda = 620$ nm). It exhibited efficiency improvement and narrower FWHMs (51 nm at 20 mA). The light output power and EQE were 0.23 mW and 0.6% at 20 mA operation. According to Yoshida *et al*, for InGaN QWs grown on sapphire substrates, the first QW grown has a large possibility to generate misfit dislocations due to the large lattice mismatch [118]. The role of the inserting blue-green single QW suggests preventing the generation of misfit dislocations in orange-red QWs. Meng *et al* also reported amber LEDs with dual-wavelength structures [119]. The emission peak wavelength was obtained at 609–591 nm with an injection current of 5–100 mA. Very recently, this same group demonstrated red LEDs using the same growth technique [120]. The small blueshift was attributed to the partial strain relaxation by the lower In content InGaN QWs. However, the FWHM was 85–94 nm, which is broader than the other reports (47–59 nm [29, 36, 117]) due to In-rich clusters.

3.2. Strain-compensating barriers

Al(Ga)N interlayers located between InGaN QWs and GaN barriers were reported to improve the efficiency of the high-In-content InGaN LEDs in the green to red spectral ranges [29, 35, 58, 121, 122]. The Al content of the Al(Ga)N interlayer increases with In content as the InGaN QW increases. For red LEDs, the Al content in Al(Ga)N interlayers were employed at >0.9 [29]. To discuss the band engineering of the QW structures, the Al(Ga)N interlayers affect the electron carrier confinement in the QW because they provide high band offset. The electron wave function will shift toward the zone center in the QW. Therefore, one benefit of Al(Ga)N interlayers is that it leads to an increase in the overlap between electron and hole wave functions. On the other hand, high-Al-content Al(Ga)N interlayers induced a tensile strain that can improve the crystal quality of InGaN QWs by strain compensation [29, 121, 123]. Also, the interlayers are helpful to suppress the In re-evaporation from InGaN QWs during the barrier layer growth due to the thermal budget.

The barrier layer's thickness and composition provided a larger strain-compensating effect than the interlayers between QWs and the barriers. Lekhal *et al* reported the behavior of the AlGaN barrier thickness for the strain-compensating effect, as shown in figure 9 [124]. The PL intensity was enhanced as the AlGaN barrier thickness increased from 1.4 to 10.6 nm. The peak emission wavelength was redshifted due to an increase in the internal electric field in the InGaN QWs. In general, the behavior of redshifting and IQE has been understood as a trade-off: The material quality of the InGaN QWs was significantly improved due to suppressed defect generation by strain compensation.

We demonstrated InGaN-based amber/orange/red LEDs using the strain-compensating barriers of Al(Ga)N [34, 35, 117, 121]. Those LEDs have enhanced EQE and narrowed FWHMs due to improved crystal quality of the InGaN QWs. The Al content in AlGaN barriers needs to be increased with the longer peak emission wavelength due to strain compensation. The disadvantage of AlN and AlGaN barrier structures is the high operation voltage (e.g. 3.3–4.5 V at ∼10 A cm^{-2} [29, 121]) due to a large barrier potential increase.

4. Growth orientation

The crystal orientations such as (000–1) N-polar and semipolar are attractive and can grow high-In-content InGaN

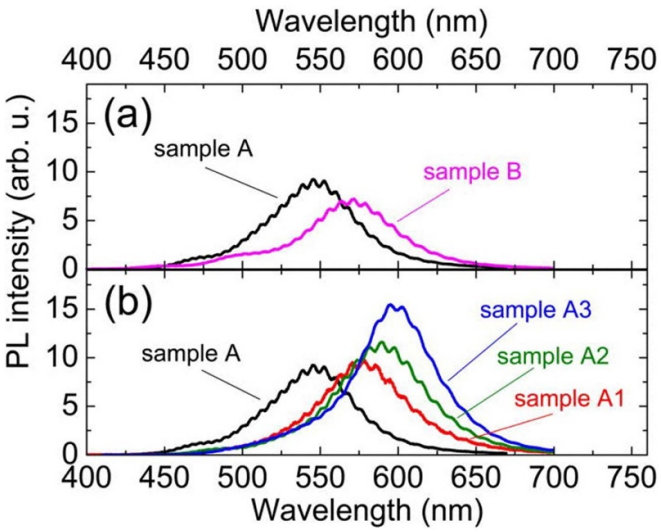

Figure 9. Room temperature photoluminescence spectra of (a) InGaN/GaN and (b) InGaN/AlGaN/GaN multiple QWs. The In content in InGaN is 0.21 (samples A, A1, A2, and A3) and 0.22 (sample B) for growth temperatures of 715 °C–700 °C. The thickness of the $Al_{0.2}Ga_{0.8}N$ increased from 0 to 1.4 nm, 5.2 nm, and 10.6 nm for samples A, A1, A2, and A3, respectively. Reprinted from [124], with the permission of AIP Publishing.

because of the much higher In incorporation compared to a conventional (0001) Ga-polar orientation [125–129]. N-polar orientation provides the reversed spontaneous and piezoelectric fields compared to conventional Ga-polar systems due to polarization engineering in the case of light-emitting devices. This orientation in turn leads to a low forward voltage and reduction in efficiency loss [130, 131]. Also, semipolar and nonpolar orientations have a significant advantage for the reduction of QCSE [132–134]. These characteristics improve the efficiency of the high-In-content InGaN light-emitting devices. We will next discuss the detailed performance of the N-polar and semipolar orientated (In)GaN growth.

4.1. (000–1) N-polar growth

N-polar growth favors In incorporation into InGaN; therefore, it can offer red emission. Shojiki *et al* demonstrated N-polar InGaN-based red LEDs grown by MOVPE owing to the high In uptake efficiency resulting in an EL intensity of 0.7 mW cm^{-2} (0.47 μW) with the peak emission wavelength of 633.4 nm at 20 mA (29 A cm^{-2}) [128]. Even though the InGaN growth temperature increases, the LED efficiency was low. Also, the 633 nm wavelength InGaN QW emissions was indicated a large FWHM of 114 nm at 20 mA suggesting that the In fluctuation occurred due to undulation and surface step bunching of GaN surfaces by misoriented off-angle species in the sapphire substrates. Thus, the development of the InGaN-based LEDs with N-polar orientation is not sufficiently progressed due to difficulties in crystal growth. For example, the (In)GaN crystalline quality is not sufficient due to dislocation density issues [135], the formation of hexagonal hillocks [136, 137], and residual impurities [138, 139]. To overcome these issues, crystal quality has improved over time using several growth techniques such as the optimization of V/III ratio [138, 140, 141], In [142], Mg [136, 143] surfactants, and misorientation angles [135, 137].

Especially, in the case of MOVPE, N-polar (In)GaN growth has suffered from high residual impurities such as C and O, which were reported over one magnitude higher than that in Ga-polar systems under the same growth condition [144, 145]. Notably, Lund *et al* reported that the residual C concentration is as low as 2×10^{16} cm^{-3} using triethylgallium (TEGa) and triethylindium (TEIn) precursors for InGaN MQWs growth [141]. They identified the residual O concentrations of 3–5 $\times$ 10^{16} cm^{-3} for N-polar InGaN. This was still much higher than 4–8 $\times$ 10^{15} cm^{-3} for Ga-polar systems. Based on this, the PL intensity of the N-polar InGaN MQWs was one magnitude lower than the Ga-polar one. This result suggests that nonradiative recombination channels were related to the metal-vacancy-oxygen complexes [146]. Ueno *et al* also demonstrated N-polar InGaN LEDs grown by PSD [147]. The crystalline quality of N-polar GaN layers indicated that the FWHM of x-ray rocking curves for (0002) and (10–12) diffractions were 313 and 394 arcsec, respectively. The FWHM values are comparable to the typical Ga-polar GaN. However, the background electron concentration of undoped N-polar GaN was available and could reduce the system to 8.5×10^{16} cm^{-3} suggesting that the O concentration was still higher than that of Ga-polar GaN. Those results suggest that the controlling of O incorporation during growth is critical to improving the IQE of InGaN QWs.

4.2. Non-c-plane growth

Semipolar and nonpolar growth can lead to highly efficient InGaN-based LEDs with a longer emission wavelength due to mitigation of QCSE in the InGaN QWs. A few works concerned with the InGaN-based amber-red LEDs grown on semipolar and nonpolar GaN have been reported. Semipolar (11–22) InGaN-based amber LEDs were grown on freestanding semipolar (11–22) GaN substrates [132] and *m*-plane patterned sapphire substrates [133]. Seo *et al* reported nonpolar (11–20) *a*-plane orange LEDs grown on *r*-plane sapphire substrates [148]. Those reports exhibited a small blueshift compared to conventional *c*-plane amber LEDs suggesting an effective suppression in QCSE.

Strain relaxation also leads to reduced piezoelectric fields. For example, the poor-crystalline quality of materials is easier for strain relaxed materials in the InGaN MQWs [118]. Kawaguchi *et al* demonstrated semipolar (20–21) InGaN-based red LEDs grown on freestanding semipolar (20–21) GaN substrates with a low forward voltage operation of 2.8 V at 20 mA [149].

Semipolar growth techniques have provided high-performance laser diode (LD) and vertical cavity surface-emitting laser including blue and green emissions [150–153]. However, the growth techniques are still very difficult to extend the emission wavelength. This suggests that semipolar growth needs further optimization of growth conditions.

5. Three-dimensional structures

Three-dimensional structures can realize high crystalline quality InGaN red LEDs. An excellent advantage of functional nanostructures such as NWs, nanopyramids, and platelets is that they offer defect-free structures and free-strain (i.e. polarization) for realizing high-performance LEDs. Those nanostructures are very attractive for light-emitting devices and have great potential to improve IQE. Three-dimensional structures can also improve the light extraction efficiency. Therefore, these nanostructures can provide an excellent platform for improving EQE. This is a very attractive way to improve the efficiency of the micro-LEDs because such bottom-up approaches can avoid nonradiative recombination by surfaces damaged during mesa etching. We will next review the nanoscale growth techniques for fabricating InGaN red LEDs.

5.1. Nanowire (NW) growth

Many efforts have been used to fabricate red emission NW structures by MBE. Kikuchi *et al* demonstrated 645 nm wavelength InGaN multiple quantum disks embedded in nanocolumns in 2004 (for convenience, equal to NWs). These were red LEDs on *n*-type (111) Si substrates and had self-assembled growth [154]. Following those nanocolumn growth techniques, several groups reported the NWs red LEDs ($\lambda = 600$–700 nm) with embedded InGaN quantum disks/dots by MBE growth [155–161].

For example, Jahangir *et al* also demonstrated 650 nm wavelength red NWs LEDs with a high IQE [155]. The post-growth NW surfaces were passivated by parylene, which led to significantly improved IQE from 10% to 52%. Nguyen *et al* proposed the InGaN/AlGaN quantum disks/dots LEDs with the AlGaN barrier shell structures. This led to a remarkable EL emission enhancement compared to typical GaN barriers [162]. One can further decrease the nonradiative surface recombination and improve the carrier injection.

Zhao *et al* demonstrated InGaN/GaN quantum-disks in NW LEDs ($\lambda = \sim$700 nm); these were self-assembled directly on metal-substrates by MBE [158, 159]. The devices obtained a light-output power as high as 8 mW at 600 mA operation. Bui *et al* also reported extremely small blueshift values operating at 50–350 mA 1.5 nm for the blue micro-LEDs and 3 nm for the red ones [160]. The blueshift behavior indicated a negligible level due to the reduced polarization field attributed to the screening of the QCSE via a high current density operation. This work also suggests that the lateral strain relief in NWs contributed to reduced polarization. Such spontaneously self-assembled NW structures will have a broad emission spectrum (FWHM: >90 nm [155, 158, 160]) because the emission wavelength and intensity varied by wire-to-wire fluctuations. This broad spectrum is favorable and can lead to phosphor-free white emission with a relatively high color rendering index.

High-performance nanostructure devices are useful for high-definition displays and must have a precise arrangement in terms of periodicity and diameter. Vadivelu *et al* first demonstrated a InGaN QWs nanocolumn with red LEDs via a selective area growth technique [156]. Figure 10 shows that

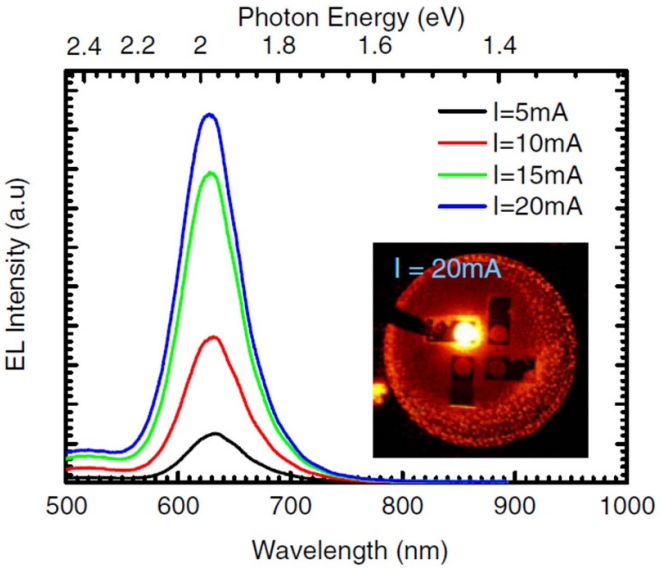

Figure 10. The EL spectra of an LED for an injection current from 5 to 20 mA (65–255 A cm^{-2}). The near field emission image at 20 mA is shown in the inset. Reproduced from [156]. © IOP Publishing Ltd. All rights reserved.

the emission peak wavelength and FWHM were 633 nm and 185 meV (∼60 nm) at 5 mA (65 A cm^{-2}), respectively. This indicates a small blueshift of 5 nm because of the high current density operation that contributes to the screening of the polarization field. It also suggests that the polarization and band filling effects are negligible due to the strain relief in the active regions. The light-output power was as low as 16 μW at 20 mA. The same group reported nanocolumns red LEDs with a very narrow FWHM of 15 nm at a 637 nm peak emission wavelength [161]. This showed that the periodic arrangement of nanocolumns architecture leads to photonic crystal effects [163]. As a result, the directional beam profile produced a small radiation angle of $\pm 30^{\circ}$ due to the light diffraction at the photonic band edge.

The selective area growth techniques for NWs are a very attractive way to fabricate the monolithic integrated three primary colors on the same wafers. Sekiguchi *et al* controlled the In content in InGaN QW via nanocolumn diameters in 2010 [164]. The emission wavelengths were controlled from blue (479 nm) to red (632 nm) with increasing diameters. The effect was explained by the beam shadowing of the neighboring nanocolumns and the adatoms diffusion length from the sidewall surfaces. The same group demonstrated integrated red, green, blue, and yellow micro-LEDs on the same wafer [165].

Ra *et al* also reported a single or a few NWs on the same LED chips with emission wavelength tunable via the NW diameter [166]. The active region was composed of InGaN QDs in NWs. The reduction in the NW diameters led increased the amount of In adatoms on the top region due to both impingent adatoms and migrated adatoms from the sidewall surfaces. These offer a longer emission wavelength. The monolithically integrated multicolor single NW LED pixels show four EL peak wavelengths based on by varied NW diameters:

659 nm (diameter: 220 nm), 625 nm (diameter: 320 nm), 526 nm (diameter: 420 nm), and 461 nm (diameter: 630 nm). These approaches are promising for the development of full-color light-emitting devices for various applications.

A few works have reported on NW red LEDs grown by MOVPE. InGaN core–shell NW LEDs grown on GaN templates use selective area growth technique and were demonstrated by Hong *et al* in 2011 [167]. Embedded InGaN QWs were anisotropically grown on the topmost plane/facet and the sidewall surfaces. The LEDs have a color-tunable emission from red to blue due to the non uniform current injection path. The red emission was obtained from the topmost InGaN QWs. The LEDs exhibited a peak emission wavelength at 680–690 nm under lower current densities (<20 A cm^{-2}).

Glō is a leading company producing nitride-based NW LEDs—they have reported InGaN core–shell NW LEDs in the orange-red spectral range. LEDs with a 600 nm peak wavelength had an estimated encapsulated EQE of approximately 3% at 0.5 A cm^{-2} [168]. Kum *et al* demonstrated excellent wafer-level uniformity of GaN NW structures on 100 mm sapphire substrates using a two-step self-limited method via MOVPE [169]. The InGaN/GaN core–shell NW LEDs were fabricated and show that the RGB emissions on the same wafer had a varied pitch for the NWs [169]. The EL peak emission wavelength was obtained at 600 nm for 65 mA (1.5 A cm^{-2}).

Recently, triangular-shaped semipolar (11–22) InGaN/GaN MQW shells in NW LEDs were grown on an amorphous glass substrate using MOCVD by Johar *et al* [170]. The high crystalline quality GaN NW growth on a glass substrate was based on catalyst-assisted growth technique including two-step growth vapor–liquid–solid and vapor–solid methods. The GaN NWs were formed along the *m*-axis orientation using a Au catalyst [171]. The red PL emission is up to 703 nm and was observed from InGaN MQW shells. The estimated IQE was as high as 35.6% via the ratio of integrated PL intensity at LT and RT. This can lead to longer emission wavelengths using InGaN QWs.

5.2. Nanopyramid and platelet structures

Another attractive way has been proposed for high-crystalline quality InGaN templates using nanostructures such as nanopyramids and platelets; these materials have great potential for high-efficiency red LEDs [172–174]. Such syntheses can take advantage of strain relaxation, low dislocation densities, and a reduction in the piezoelectric field. In turn, the InGaN QWs on those nanostructures can improve IQE. Chang *et al* reported a 600 nm wavelength amber LED on nanopyramid GaN structures [175]. The IQE was as high as 21%. However, the amber LEDs had no EL emission until 40 mA due to a considerable current leakage due to defects on the coalesced pyramid boundaries. Ko *et al* demonstrated a 650 nm emission InGaN double heterostructure grown on GaN nanopyramids. This system formed semipolar facet planes using an MOVPE selective area growth method with nanoimprinting [174]. The role of nanopyramid structures is to grow high-In-content InGaN owing to the surface diffusion of adatoms and the compositional pulling effect. This is a very interesting approach to obtain red emission. Very crystalline nanopyramids offer good IQE improvements of 0.56%–7.2% compared to the planar structures.

InGaN nanopyramid structures have been proposed as templates for the growth of high-In-content LEDs. To realize highly selective InGaN growth on GaN templates with dielectric-masked nano-holes, a pulse interruption of Ga precursors was introduced during InGaN growth [176, 177]. Several groups have reported the fabrication of high-crystalline quality InGaN hexagonal nanopyramid structures with a relatively high In content using a nanoscale selective area during MOVPE growth [174, 178–180]. GaN nuclei growth during opening of nano-holes is essential to obtaining precisely controlled InGaN pyramids [177, 178]. The InGaN nanopyramids showed six smooth sidewall semipolar facets corresponding to {10–11} planes. The nanopyramid structures were dislocation-free because the window area was very small (100 nm diameter) to induce elastic strain relaxation. This growth technique is an attractive way to obtain high-quality crystals and very homogeneous InGaN nanostructures for red LEDs.

Bi *et al* demonstrated high-crystalline quality InGaN platelets combined with selective area MOVPE growth and *in situ* annealing process [173]. Figure 11 shows the procedure for InGaN-based LED grown on platelet structures [173]. The *in situ* annealing process provided *c*-plane surfaces formed by etching down from the InGaN pyramid apex. The LED structures were grown on those InGaN platelets. Notably, the FWHM of red LEDs was very narrow and as low as 48 nm (150 meV); there was no blueshift with current increases as shown in figure 11(g). To further improve the crystalline quality of InGaN platelets, InGaN pyramids were polished from the apex by a chemical mechanical polishing technique [172]. In this way, the InGaN platelet is not required to grow InGaN layers with intermediate to low In contents—this prevents the generation of dislocations due to lattice mismatch. Such strain-relaxed InGaN platelets are a new platform for high-In-content InGaN light-emitting devices and are superior to develop the application for micro-LED displays.

5.3. Quantum dots (QDs)

Conventional InGaN active regions consist of QW structures but QDs can also facilitate red emission. The QD-active regions can improve the crystalline quality of high-In-content InGaN and reduce QCSE by strain relaxation compared to conventional QW structures. In general, the QD-active region provides superior advantages such as stronger quantum confinement [181–183], carrier localization [184, 185], short radiative carrier lifetime [186], high wavelength stability [182, 183, 186], and high temperature stability of emissions [182, 184].

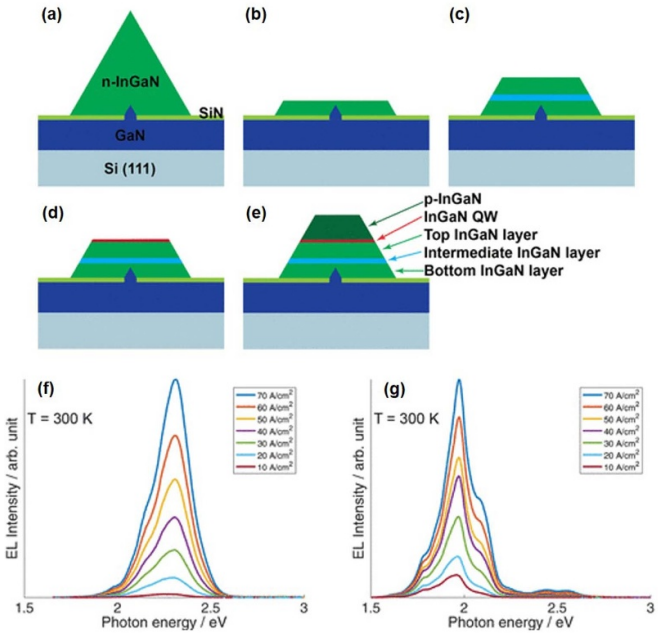

Figure 11. Procedures to synthesize InGaN platelets and LED structures. (a) InGaN pyramids grown by selective area MOVPE. (b) Bottom InGaN layer with a top *c*-plane formed by etching down from the pyramid apex using *in situ* annealing. (c) InGaN regrowth to flatten the rough *c*-plane formed in panel b. An intermediate layer of InGaN is grown first with an indium content of <5%. A top InGaN layer is then grown with an indium content similar to that of the bottom InGaN layer in panel b. (d) InGaN single QW growth on the *c*-plane of the InGaN platelet templates. (e) Prototype LED structure with *p*-InGaN grown above the single QW with definitions of all InGaN layers. (f), (g) EL spectra obtained at different current injection levels for the green LEDs grown on $In_{0.09}Ga_{0.91}N$ platelets and the red ones on $In_{0.18}Ga_{0.82}N$ platelets, respectively. The current density in both legends was calculated according to the actual QW area rather than the contact area. Reprinted with permission from [173]. Copyright (2019) American Chemical Society.

The red LEDs with self-assembled InGaN QDs with InGaN wetting layers were formed via the Stranski–Krastanov (SK) growth mode. InGaN QDs red LEDs with composite InGaN/AlN/GaN active regions were formed by TMIn treatment of the wetting InGaN layers with a peak emission wavelength of 661 nm at 60 mA [187]. The InGaN QDs were obtained via a growth interruption method. The emission peak wavelength was 729 nm at 80 mA [188]. The composite InGaN/GaN structures were formed by phase-separation due to surface roughness of the underlying *n*-GaN layer; emission was at 610 nm [189]. QD-like clusters formed into InGaN QWs due to InGaN phase-separation, which indicated red emission at 620 nm at 20 mA [184]. The blueshift behavior was only 2 nm with current injection from 40 to 100 mA. This suggests that the QCSE in such QD structures is suppressed by strain relaxation. Very recently year, Wang *et al* reported near-ultraviolet to red LEDs with Volmer–Weber (VW) InGaN QDs by MOVPE [186]. The carrier lifetime of VW QDs was much shorter than SK ones. This property is very attractive for visible light communication applications.

6. A unique approach for red emission by Eu-doping

An alternative approach has been proposed for red emissions from Eu-doped GaN active layers [190]. The $^5D_0$–$^7F_2$ transition of the 4 f shell in Eu^{3+} ions is known as the ∼621 nm emission with an ultra-narrow FWHM of ∼1 nm [190]. This is a very attractive optical property for display applications compared to typical InGaN red LEDs that have a FWHM as large as 50 nm [29]. Also, the GaN:Eu active layers do not suffer from the QCSE issue, therefore, the emission peak wavelengths can be stabilized.

To date, many efforts have been reported for Eu-doped GaN fabrication of high-purity red-emitting systems such as a ion implantation with post-thermal annealing [191, 192], MBE [190, 193–200], and MOVPE [200–207]. Co-doping into GaN:Eu have been proposed to improve the efficiency of the red emissions. Takagi *et al* demonstrated a drastic Eu luminescence enhancement of 20 fold via Mg co-doping [196]. The same group also reported that the Mg co-doped GaN:Eu nanocolumns using red LEDs had feasible crystal quality even though there was heavy Eu doping at up to 6×10^{20} cm^{-3} [200].

Lee *et al* demonstrated that Mg–Si–Eu co-doping in GaN provided a new Eu luminescence with stable thermal annealing in an ambient N_2 environment [208]. Mitchell *et al* reported the utilization of O co-doping into GaN:Eu, which increased the homogeneity of Eu incorporation into Ga-sites without Eu precipitation on the surface [203, 209]. These techniques led to the formation of new Eu centers related to Mg or O. This improves the energy transfer efficiency. Co-doping is an important technique to create high-performance GaN:Eu-based red LEDs with controlled Eu ion luminescence centers.

Fujiwara's group demonstrated the low forward voltage operation of GaN:Eu-based red LEDs using MOVPE in 2009 [207]. By further optimizing the growth conditions such as growth pressure [206], growth temperature [202], V/III ratio [204], multilayer structure [201, 209], and co-doping [203, 209], GaN:Eu-based red LEDs achieved a light-output power of 1.25 mW at 20 mA. This was an EQE of 3.3%, as shown in figure 12 [209]. The maximum EQE was as high as 9.2%. The device features are comparable with InGaN-based red LEDs.

Fujiwara's group first demonstrated monolithically integrated RGB LEDs with InGaN QWs and GaN:Eu,O active layers [23]. Notably, the optical properties such as blueshift and FWHM behaviors of GaN:Eu,O LEDs were remarkably stabilized by current injection compared to InGaN-based LEDs. The GaN:Eu LEDs had 100% purity of the 621 nm wavelength red emission due to the ultra-narrow FWHM of ∼1 nm. The RGB LEDs had a high coverage of 91.2% of the Rec. 2020

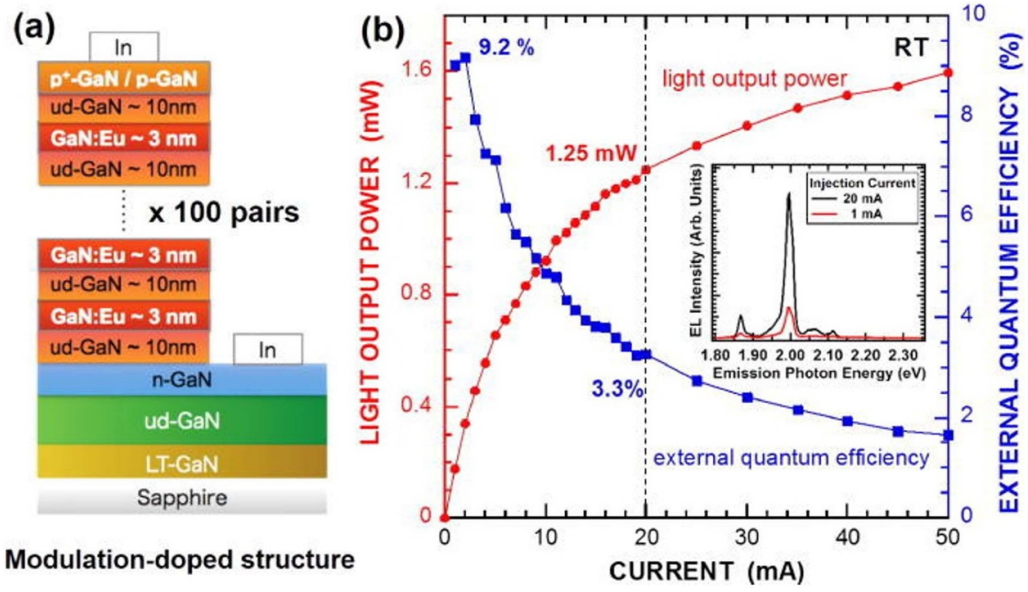

Figure 12. (a) Schematic of an LED with an active layer comprised of 100 pairs of alternating GaN and GaN:Eu layers. (b) The output power and EQE of this LED is plotted as a function of injection current. The maximum output power at 20 mA, was 1.25 mW, and the maximum EQE was 9.2% at 2 mA. The inset shows the emission spectra from this LED at two different injection currents. Reprinted from [209], with the permission of AIP Publishing.

standard in CIE 1931. This way is favorable and can realize high pixel density micro-LED applications.

7. Device characterizations

This chapter describes the device performance of (In)GaN-based LED at longer emission wavelengths in the range of yellow to red. We review state-of-the-art performance features such as EQEs, FWHMs, blueshifts, and thermal stability in (In)GaN-based LEDs.

7.1. EQE in InGaN-based red LEDs

This section summarizes the characteristics of the InGaN-based LEDs with emission longer than 580 nm (tables 2–4). Figure 13 describes the EQE as a function of the peak emission wavelength. The light extraction efficiency is not the same between each publication because efficiency is quite sensitive to device configuration (resin packaging, surface roughening, and patterned sapphire substrates). Device size could also be influenced by the IQE due to SRH nonradiative recombination [14].

In 2013, the Toshiba company first demonstrated 629 nm wavelength InGaN-based red LEDs with light-output power exceeding 1 mW at 20 mA ($\sim$10 A cm^{-2}) [29]. The EQE was as high as 2.9%. They adopted the AlGaN interlayer in the active regions to improve the crystalline quality of InGaN QWs and increase the overlap between electron and hole wave functions. However, this structure suffers from disadvantages such as high forward voltage operation (4.4 V at 20 mA), which negatively affects WPE.

Recently, the Nanchang University group demonstrated a peak WPE of orange-red LEDs that was as high as 24.0% at a low current density (0.8 A cm^{-2} at 2.0 V) [36]. The LEDs utilized GaN on Si, which led to improved crystalline quality of InGaN via growth based on temperature increases. They adopted V-pit structures that improved hole injection to obtain a low forward voltage operation. When comparing these data (table 2), the operation current density should be closely maintained because most of the reported EQE values are given by a current density of 10–30 A cm^{-2}. Devices will blueshift (ca. 20–30 nm) and efficiency will decrease at high current density operations ($\geqslant$10 A cm^{-2}) due to polarization effects, Auger recombination, and current leakage. Also, the same group reported the 585 nm wavelength yellow LEDs with a EQE of 12.6% at 20 A cm^{-2} [104]. These findings suggest that the efficiency trend is similar to Toshiba's result when the devices operate at a high current density.

These efforts have contributed to improved efficiency of the LEDs. Nevertheless, the EQEs of state-of-the-art InGaN-based red LEDs are far worse than conventional blue and green LED systems. The low-efficiency obstacle with InGaN-based red LEDs is a large QCSE and a low-crystalline quality in the active regions. This means that the red LEDs need further progress in the growth methods mentioned in sections 2–3; breakthrough growth techniques are needed.

7.2. Spectral characteristics

In this section, we report details of the spectral characteristics of InGaN-based red LEDs. The FWHMs of emission spectra are a critical parameter to govern the apparent colors of InGaN-based red LEDs. Figure 14 shows the FHWMs of InGaN-based LEDs with various peak emission wavelengths listed in tables 2–4. The FWHM values tend to be larger with

Table 2. Structures and characteristics of the reported (0001) *c*-plane (In)GaN-based LEDs with yellow to red emission. Most LEDs were grown by MOVPE but one used a PSD method. The EQE values were obtained by on-wafer testing when the device area was 50×50 μm^2 or smaller.

Year	Affiliation	Active region	Substrate	λ_{peak} (nm)	I (mA)	Device area ($\mu m \times \mu m$)	EQE (%)	FWHM (nm)	Reference
1998	Nichia	2.5 nm InGaN SQW	Sapphire	594	20	350×350	3.35	50	[210]
1999	Nichia	6 nm InGaN SQW	Sapphire	675	20	350×350	0.82	—	[28]
2002	Nichia	3 nm InGaN SQW	Sapphire	631	20	350×350	1.1	—	[211]
2006	National Taiwan Univ.	InGaN/GaN 5QWs	Sapphire	600	20	300×300	—	57	[212]
2012	Tokyo Univ. of Science	InGaN/(In)GaN 16QWs	Sapphire	740	20	500×500	—	138	[56]
2014	Toshiba	$In_{0.35}Ga_{0.65}N$/AlGaN/InGaN 4QWs	PSS	629	20	460×460	2.9	53	[29]
2014	The Univ. of Tokyo	30 nm $In_{0.33}Ga_{0.67}N$	Graphene/SiO_2	640	20	—	—	60	[213]
2015	Chinese Academy of Sciences	InGaN/GaN 5QWs	Sapphire	585	50	500×1000	1.4	—	[214]
2016	Tokyo Univ. of Science	InGaN/AlN/GaN/AlGaN/GaN 2QWs	Sapphire	600	20	370×370	0.8	50	[121]
2016	Tokyo Univ. of Science	InGaN/AlN/GaN/AlGaN/GaN 2QWs	Sapphire	620	20	370×370	0.6	51	[117]
2016	Tokyo Univ. of Science	InGaN/AlN/GaN/AlGaN/GaN 2QWs	Sapphire	631	20	370×370	0.4	52	[117]
2017	Chonbuk National Univ.	$In_{0.45}Ga_{0.55}N/In_{0.13}Ga_{0.87}N$ 5QWs	PSS	596	80	—	—	69	[215]
2017	Chonbuk National Univ.	$In_{0.42}Ga_{0.58}N/In_{0.13}Ga_{0.87}N$ 5QWs	PSS	597	20	1000×1000	1.2	62	[216]
2017	Osaka Univ.	GaN:Eu	Sapphire	621	20	—	0.94	~1	[201]
2018	Osaka Univ.	GaN:Eu	Sapphire	621	20	—	3.3	~1	[209]
2019	Nanchang Univ.	InGaN/GaN 8QWs	Si (111)	585	200	1000×1000	12.6	48.6	[104]
2019	Chinese Academy of Sciences	InGaN/GaN 2QWs	PSS	603	20	—	—	75	[119]
2020	Univ. of Grenoble-Alpes	$In_yGa_{1-y}N/In_xGa_{1-x}N$ 5QWs	InGaNOS	620	11	300×300	—	67	[77]
2020	Univ. of Grenoble-Alpes	$In_yGa_{1-y}N/In_xGa_{1-x}N$ 5QWs	InGaNOS	623	0.3	50×50	—	58	[77]
2020	Univ. of Grenoble-Alpes	$In_yGa_{1-y}N/In_xGa_{1-x}N$ 5QWs	InGaNOS	612	15.3	300×300	0.01 (on wafer)	—	[77]
2020	Univ. of Grenoble-Alpes	$In_yGa_{1-y}N/In_xGa_{1-x}N$ 5QWs	InGaNOS	616	1	50×50	0.09 (on wafer)	—	[77]
2020	KAUST	InGaN/AlN/GaN/AlGaN/GaN 2QWs	PSS	633	20	400×400	1.6	59	[35]
2020	KAUST	InGaN/AlN/GaN/AlGaN/GaN 2QWs	(−201) β-Ga_2O_3	665	20	650×250	0.19	67	[34]
2020	Nanchang Univ.	InGaN/GaN 2QWs	Si (111)	608	8	1000×1000	23.5	43.5	[36]
2021	UCSB	InGaN/AlGaN/GaN 3QWs	InGaN on porous GaN/sapphire	632	0.004	6×6	0.2 (on wafer)	62	[74]
2021	Chinese Academy of Sciences	InGaN/GaN 2QWs	PSS	615	20	—	—	87	[120]
2021	KAUST	InGaN/AlN/GaN/AlGaN/GaN 2QWs	PSS	626	0.09	47×47	0.36 (on wafer)	52	[24]
2021	KAUST	InGaN/AlN/GaN/AlGaN/GaN 2QWs	PSS	606	0.44	47×47	0.56 (on wafer)	50	[217]

Table 3. Structures and characteristics of the reported semipolar, nonpolar, and (000–1) N-polar orientated InGaN-based LEDs with yellow to red emission.

Year	Affiliation	Growth method	Active region	Orientation	λ_{peak} (nm)	I (mA)	Device area (μm × μm), or diameter (μm) or emission area	EQE (%)	FWHM (nm)	Reference
2006	Kyoto Univ.	MOVPE	3 nm InGaN/GaN SQW	(11–22)	590	20	320 × 320	1.3	53	[132]
2011	Korea Electronics Technology Institute	MOVPE	18 nm InGaN/GaN SQW	(11–20)	612.2	20	200 × 500	—	72	[148]
2013	UCSB	MOVPE	3 nm InGaN/GaN SQW	(20–21)	624	20	340	—	—	[149]
2015	Univ. of Sheffield	MOVPE	InGaN/GaN SQW	(11–22)	584	20	330 × 330	—	70	[133]
2015	Univ. of Sheffield	MOVPE	InGaN/GaN SQW	(11–22)	608	20	330 × 330	—	—	[133]
2015	Univ. of Sheffield	MOVPE	InGaN/GaN SQW	(11–22)	594	100	330 × 330	—	88	[133]
2015	Tohoku Univ.	MOVPE	InGaN/GaN 5QWs	(000–1)	633.4	20	67 600 μm^2	—	114	[128]
2015	Tohoku Univ.	MOVPE	InGaN/GaN 5QWs	(000–1)	600.5	20	67 600 μm^2	—	97	[128]
2017	The Univ. of Tokyo	PSD	10 nm $In_{0.4}Ga_{0.6}N$	(000–1)	609	20	—	—	94	[147]

a longer peak emission wavelength. This is a typical phenomenon of InGaN-based LEDs, which can be described by an energy potential distribution due to disordered alloy compositions and thicknesses. Strain relaxation causes the InGaN active regions to induce inhomogeneous In incorporation via defects (dislocations and trench defects) [121]. Residual strain can propagate from patterned substrates to induce a wide distribution of In content and QCSE [218]. Therefore, the FWHM behaviors depend on the configuration of the device structures such as growth orientations, design of active regions, patterning of substrates, and dimensions.

Semipolar and nonpolar orientations are required for larger In content in InGaN QWs compared to *c*-plane systems because of a low QCSE. This presumes a high possibility of generating defects due to the strain relaxation, which induces disordered In incorporation into InGaN-active regions. The FWHMs of (000–1) *c*-plane LEDs are as large as the (0001) *c*-plane systems. The origin of broad spectra of (000–1) *c*-plane LEDs is large In fluctuations and QW thickness disorders due to step bunching and surface undulation [135, 141, 219]. The misorientation angles of substrates are associated with those issues. Meanwhile, the disorder of In incorporation (phase separation) is due to the In-rich InGaN QD structures leading to red emissions. However, based on the reason above, the FWHMs of QD structures increase drastically compared to that of conventional QW structures. InGaN nanostructured devices such as NWs and InGaN platelets were formed by spontaneous self-assembly or controlled mask-patterned growth methods. In incorporation is very sensitive to the diameter of the nanostructures [164, 166]. Therefore, the emission of spontaneously self-assembled random nanostructures becomes broad due to wire-to-wire fluctuations compared to that of controlled ones.

The hue of InGaN QWs emission is determined by the peak wavelengths and their FWHMs. The hue of the InGaN red QWs emission is not matched with its peak emission wavelength due to the broad spectra. Robin *et al* reported on the hue of InGaN QWs emission in the red spectral range. The red spectral range can be obtained via high color saturation even with large FWHMs [25]. However, the broad spectra led to a large hue blueshift over 575 nm emission—this is known as the Abney effect; the hue of monochromatic light can be affected by bandwidth. Mizokami *et al* reported on the relationship between emission wavelength and its bandwidth for estimating the Abney effect [220]. Figure 14 shows the wavelength tendency according to the Abney effect. The hue of the emission wavelength (apparent wavelength) depends on its FWHMs. According to the Rec. 2020 standard, primary red, green, and blue colors are located at (0.708, 0.292), (0.17, 0.797), and (0.131, 0.046) in Commission Internationale de l'Eclairage (CIE) 1931 chromaticity coordinates, respectively. Thus, it requires red emission whose apparent wavelength is 630 nm.

To realize the apparent emission wavelength at 630 nm for the Rec. 2020 standard, current reports suggest that InGaN-based red LEDs are required to emit at a peak wavelength over 660 nm. The broad spectra are obstacles to realizing highly-efficiency LEDs with a pure red emission. Some InGaN-based red LEDs have been reported in an unexpected additional short-wavelength peak emission attributed to the InGaN phase-separation in the active regions [28, 29, 35, 77, 121]. This issue is affected by the color saturation of the LEDs.

Table 4. Structures and characteristics of the reported nanostructured InGaN-based LEDs with yellow to red emission.

Year	Affiliation	Growth method	Active region	Array nano structure	λ_{peak} (nm)	I (mA)	Device area (μm × μm), or diameter (μm) or surface area	FWHM (nm)	EQE (%)	Reference
2007	Boston Univ.	MBE	InGaN/GaN QDs	Random	640	20	—	97	—	[222]
2010	A* STAR, National Univ. of Singapore	MOVPE	InGaN/AlN/GaN QDs	Random	582	30	—	57	—	[223]
2010	A* STAR, National Univ. of Singapore	MOVPE	InGaN/AlN/GaN QDs	Random	617	30	—	99	—	[223]
2011	A* STAR, National Univ. of Singapore	MOVPE	InGaN/AlN/GaN QDs	Random	661	60	—	120	—	[187]
2011	Yeungnam Univ.	MOVPE	30 nm InGaN QDs	Random	610	20	300 × 300	75	—	[189]
2012	McGill Univ.	MBE	InGaN/GaN QDs in NWs	Random	652	50	500 × 500	90	—	[224]
2013	Sophia Univ.	MBE	InGaN/GaN 3QWs in NWs	Controlled	597	10	65	54	—	[225]
2013	Univ. of Michigan, OSRAM	MBE	$In_{0.54}Ga_{0.46}N$ quantum disks in NWs	Random	650	30	7.8×10^{-4} cm^{-2}	95	—	[155]
2013	National Chiao Tung Univ.	MOVPE	Nanopyramid InGaN/GaN MQWs	Controlled	645	50	300 × 300	119	—	[175]
2013	Tsinghua Univ.	MOVPE	InGaN/GaN QDs	Random	738	75	300 × 300	112	—	[188]
2013	Tsinghua Univ.	MOVPE	InGaN/GaN QDs	Random	708	100	300 × 300	145	—	[188]
2013	Sophia Univ.	MBE	InGaN/GaN 3QWs in NWs	Controlled	633	5	100	60	—	[156]
2014	Univ. of Michigan, OSRAM	MBE	$In_{0.51}Ga_{0.49}N$ quantum disks in NWs	Random	610	—	—	74	—	[157]
2015	Sophia Univ.	MBE	InGaN/GaN 5QWs in NWs	Controlled	670	10	65	62	0.07	[226]
2016	McGill Univ., McMaster Univ., Samsung	MBE	InGaN/GaN QDs in NWs	Controlled	659	4.5×10^{-3}	0.22	103	—	[166]
2016	McGill Univ., McMaster Univ., Samsung	MBE	InGaN/GaN QDs in NWs	Controlled	625	4.5×10^{-3}	0.32	72	—	[166]
2016	KAUST	MBE	InGaN quantum disks in NWs	Random	710	350	400	—	0.7	[158]
2016	KAUST	MBE	InGaN quantum disks in NWs	Random	705	400	200	—	0.2	[159]
2017	New Jersey Institute of Technology	MBE	InGaN/AlGaN QDs in NWs	Random	645	400	300 × 300	125	—	[227]
2018	Chinese Academy of Sciences	MOVPE	Shell- and QD-like clusters in MQWs	Random	619	20	—	85	—	[184]
2019	Lund Univ.	MOVPE	InGaN SQW in InGaN platelet	Controlled	626	∼70	360	48	—	[173]
2019	New Jersey Institute of Technology	MBE	InGaN/AlGaN QDs in NWs	Random	645	100	50	93	—	[160]
2019	Sophia Univ.	MBE	120 nm InGaN in NWs	Controlled	637	10	100	15	—	[161]
2020	Sophia Univ.	MBE	70 nm InGaN in NWs	Controlled	647	0.8	5 × 5	112	—	[165]

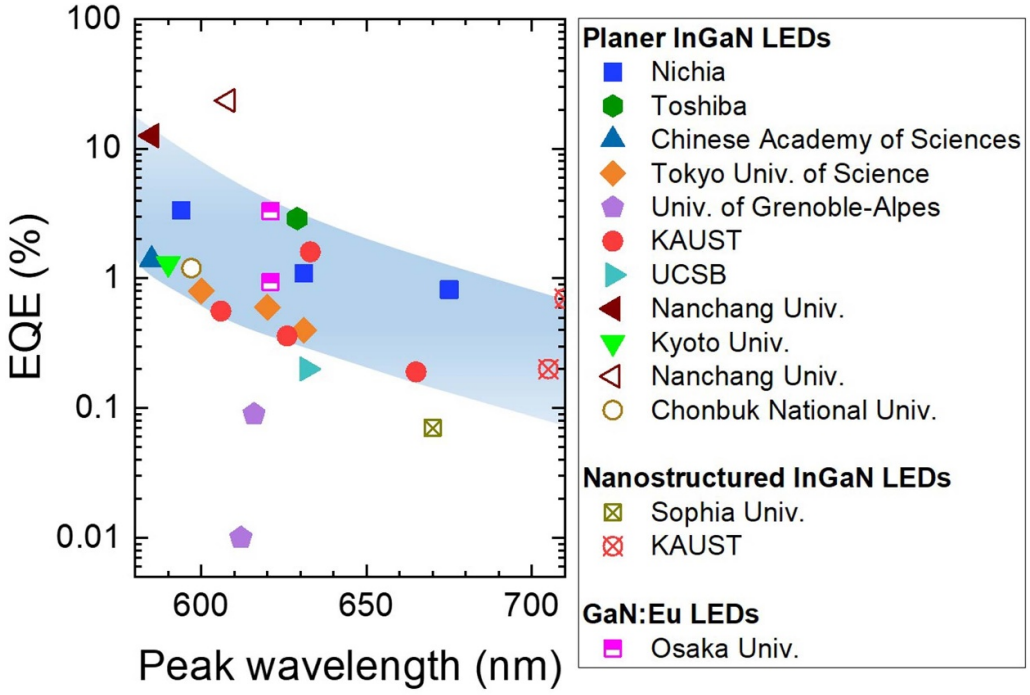

Figure 13. EQE of (In)GaN-based LEDs with peak wavelength ranges from 580 to 710 nm. Solid and open symbols are given by high ($\geqslant$10 A cm^{-2}) and low (<10 A cm^{-2}) current densities for planar InGaN LEDs, respectively. The other data correspond to nanostructured InGaN LEDs and GaN:Eu LEDs. The shaded area indicates the general trend between efficiencies and peak wavelength at standard current density ($\geqslant$10 A cm^{-2}).

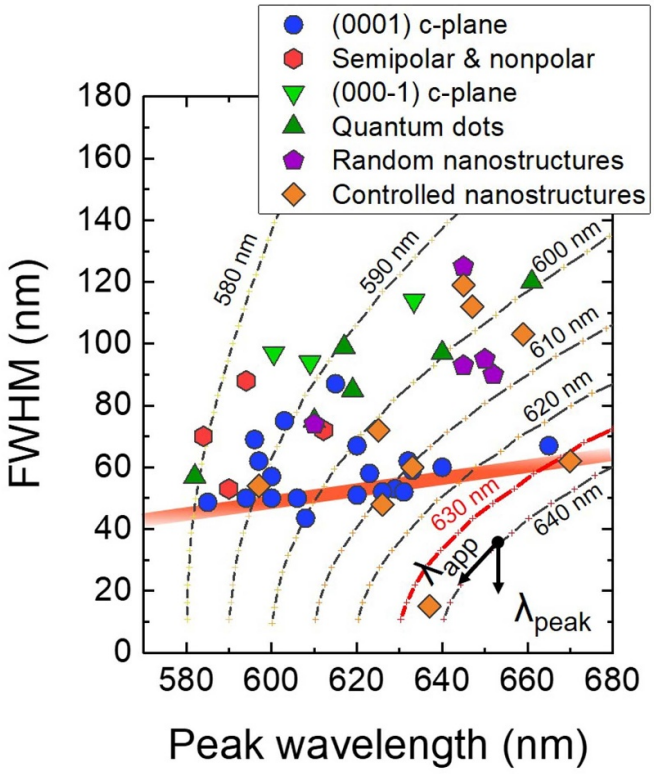

Figure 14. FWHM of InGaN-based LEDs as a function of the peak wavelength. Dashed lines correspond to the apparent wavelength (λ_{app}) which corresponds to the hue in the CIE diagram according to [220]. The red belt is a guide for the eye.

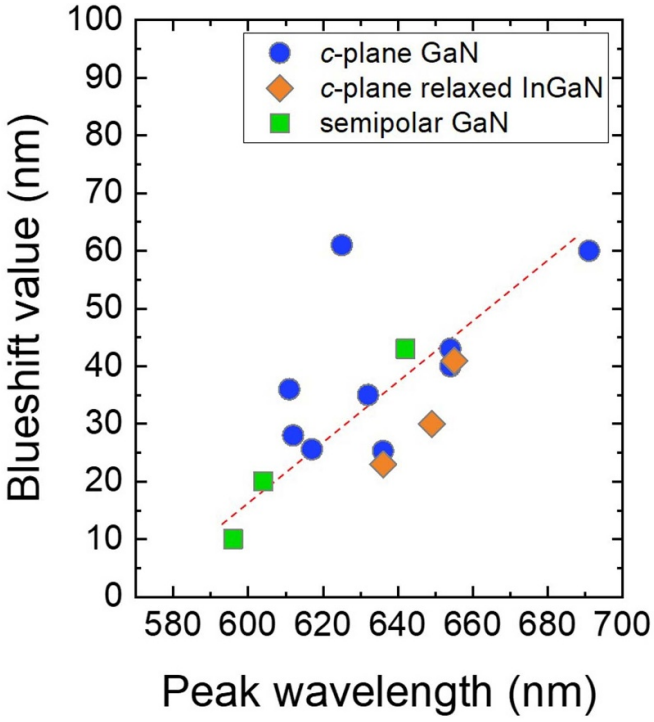

Figure 15. Blueshift behavior of InGaN-based LEDs with an orange-red spectral range. Blueshift values of the EL emissions explained differences in peak wavelengths between low (0.1–3 A cm^{-2}) and high (10–63 A cm^{-2}) current densities. Peak wavelengths are obtained at low current densities (0.1–3 A cm^{-2}). The dashed line is a guide for the eye.

The minimum FWHM range of the red LEDs at 629 nm peak emission is 53 nm corresponding to ∼166 meV [29]. In contrast, the FWHM of conventional InGaN-based blue LEDs is as small as ∼20 nm and corresponds to ∼120 meV [221]. For example, it is possible for the FWHMs of red LEDs to be the same as the energy distribution of blue LEDs. In this case, the 630 nm apparent wavelength can satisfy the red color in the Rec. 2020 standard, which requires a peak wavelength over 640 nm with a FWHM of 40 nm. Therefore, to achieve high-efficiency InGaN-based LEDs with a pure red emission, it is essential to narrow the FWHMs of the emission spectra.

In general, the peak emission wavelengths of InGaN LEDs are shifted to shorter wavelength. Current injection increases due to screening of the QCSE and band filling of localized states. This phenomenon remarkably occurs when the In content in InGaN QWs increases. Figure 15 shows this blueshifting behavior of InGaN-based LEDs in the orange-red spectral range including the polar and semipolar orientations listed in table 5. The blueshift values are quantified as the peak wavelength differences between low (0.1–3 A cm^{-2}) and high (10–63 A cm^{-2}) current densities. Semipolar LEDs can have a minimized blueshift of the peak wavelength based on the reduction of the QCSE. Bai *et al* reported a blueshift as small as 10 nm at 596 nm with increasing injection current from 1 mA (∼1 A cm^{-2}) to 50 mA (∼46 A cm^{-2}) [133]. However, the blueshift value was similar to *c*-plane LEDs at 640 nm, which suggests significant band filling of localized states due to large In fluctuation. Here, the red LEDs grown on Si substrates can have a reduced QCSE due to the strain reduction in the active region by V-pit structures. The strain-reduced InGaN QWs grown on novel InGaN templates can be mitigated by peak emission shifts via a small QCSE.

7.3. Temperature stabilities

Here, we discuss the thermal properties of InGaN-based red LEDs. It is well known that the temperature dependence of the EL measurement is an approach to study the reliability of LEDs. The increasing temperature degrades the light-output power, lifetime, and wavelength stability of LEDs. The EL intensities of LEDs usually decrease with temperature increases, i.e. thermal droop [228]. The thermal droops of EL intensity are described by [229]:

$$I = I_{T=\mathrm{RT}} \exp\left(-\frac{T-\mathrm{RT}}{T_{\mathrm{ch}}}\right), \tag{1}$$

where I is the EL intensity, $I_{T=\mathrm{RT}}$ is the EL intensity at room temperature (RT), T [K] is the temperature of the sampling stage, and T_{ch} [K] is the characteristic temperature. The characteristic temperature is a standard quantitative parameter to evaluate the temperature stability of the LEDs' EL intensity. A larger characteristic temperature implies better temperature stability of EL intensities. Figure 16(a) presents the characteristic temperatures of InGaN-based red LEDs at various current densities [24, 29, 34, 217, 230, 231]. For comparison, we also plot the characteristic temperatures of AlGaInP-based LEDs [232, 233]. We explained the characteristic temperature by the

Table 5. Blueshifts of the reported (0001) *c*-plane and semipolar orientated InGaN-based LEDs with yellow to red emission. The peak wavelengths were quantified at 0.1–3 A cm^{-2}.

Year	Affiliation	Orientation	Substrate	λ_{peak} at J = 0.1–3 A cm^{-2} (nm)	Blueshift (nm)	Reference
2006	Kyoto Univ.	(11–22)	GaN sub.	604	20	[132]
2014	Toshiba	(0001)	*c*-plane PSS	654	43	[29]
2015	Chinese Academy of Sciences	(0001)	*c*-plane PSS	611	36	[214]
2015	University of Sheffield	(11–22)	*m*-plane sapphire	642	43	[133]
2015	University of Sheffield	(11–22)	*m*-plane sapphire	596	10	[133]
2016	Tokyo Univ. of Science	(0001)	*c*-plane sapphire	617	25.6	[121]
2016	Tokyo Univ. of Science	(0001)	*c*-plane sapphire	636	25.3	[117]
2017	Chonbuk National Univ.	(0001)	*c*-plane PSS	625	61	[216]
2020	Univ. of Grenoble-Alpes	(0001)	InGaNOS	636	23	[77]
2020	Univ. of Grenoble-Alpes	(0001)	InGaNOS	649	30	[77]
2020	KAUST	(0001)	*c*-plane PSS	654	40	[35]
2020	KAUST	(0001)	(−201) β-Ga_2O_3	691	60	[34]
2020	Nanchang Univ.	(0001)	Si(111)	612	28	[36]
2021	UCSB	(0001)	InGaN on porous GaN/ *c*-plane sapphire	655	41	[74]
2021	KAUST	(0001)	*c*-plane PSS	632	35	[24]

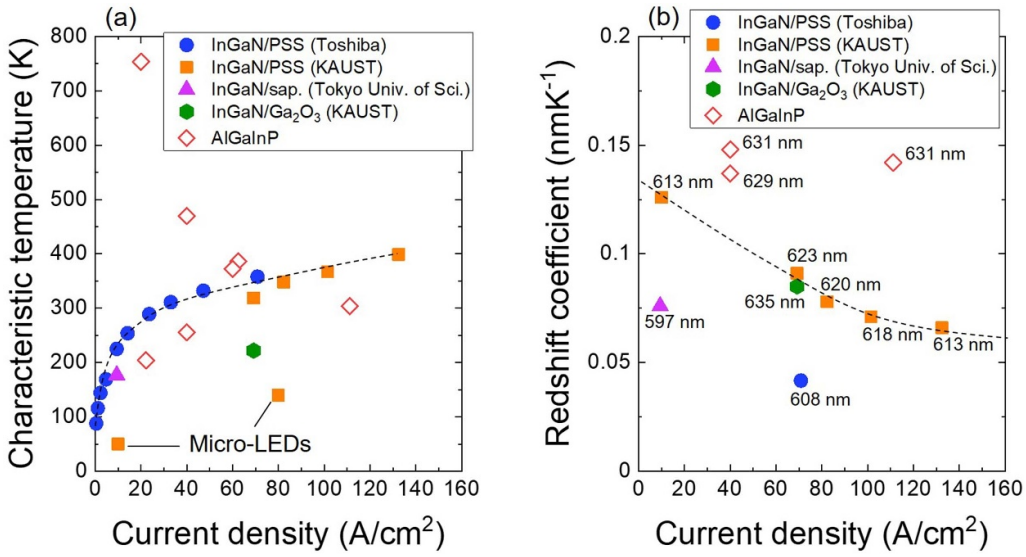

Figure 16. (a) Characteristic temperatures of InGaN- and AlGaInP-based red LEDs at various current densities. (b) Redshift coefficients of those red LEDs as a function of various current densities. The peak emission wavelengths at RT are shown. AlGaInP-based LEDs were studied under a pulse injection current. The dashed lines are a guide for the eye.

SRH nonradiative recombination [228] and carrier overflow. Note that the structures of InGaN-active regions are usually composed of a large band offset between the QWs and barriers, which probably implies a small carrier overflow. InGaN red LEDs exhibited increasing characteristic temperatures with increasing current densities suggesting that the nonradiative recombination centers play a key role in the total recombination. This phenomenon originated from the material quality and its polarization effect because of high-In-content InGaN active regions. At a low current density, those issues are significantly affected, and the characteristic temperature of InGaN is much worse than AlGaInP ones. Due to the SRH recombination process, the nonradiative recombination centers can be mitigated by high current injection, which indicates that the benefit of InGaN red LEDs in terms of temperature stability compared to the AlGaInP materials. The characteristic temperatures of micro-LEDs is low compared to standard LEDs [24, 217]. Micro-LEDs are significantly affected by temperature via non-radiative recombination centers on the sidewall surfaces.

In general, the peak wavelength of the InGaN-based red LEDs redshifts when the temperature is increased. This can be explained by the decrease in bandgap energy of the materials due to temperature increases. The redshift coefficients can be obtained by the temperature dependence of the EL measurement. The redshift coefficient of InGaN-based LEDs

[24, 29, 34, 230, 231] was smaller than that of AlGaInP ones [232, 233] (see figure 16(b)). The energy distribution of carriers in InGaN QWs transferred to high energy levels with temperature increases, which results in a blueshift of the peak wavelength [234]. This phenomenon may partially compensate for the redshift of the peak wavelength.

We also observed that the redshift coefficient reduced when the current density increased. The energy distribution of carriers at a high current density could be increased due to heat generation by a non-radiative recombination process [132], which mostly corresponded to a broadening of emission spectra toward the high energy side according to Chhajed *et al* [229]. The energy distribution of carriers at a high current density leads to blueshifting of the peak wavelength, which compensates for the redshift of the peak wavelength due to reduced bandgap energy. These results suggest that the redshift behavior originated from InGaN-active regions such as crystalline quality, thickness, compositional fluctuation, and barrier materials.

8. Conclusion

We reviewed recent progress in the development of red LEDs by III-nitride semiconductors. The critical issues of the current InGaN-based red LEDs are crystalline quality and strain of InGaN active regions. The state-of-the-art of red LEDs performance is still much worse than conventional blue and green LEDs. Further improvements in InGaN-based red LED performance can explore breakthroughs in InGaN crystal growth. We summarized trends in the development of red LEDs by III-nitride semiconductors. The growth conditions required for high-In-content InGaN are extreme. Reactor design and simulation are required to develop a high-In-content InGaN for high-temperature growth. The strain compensating technique is helpful to improve the crystalline quality of InGaN active regions. Also, unique InGaN templates or nanostructures are required to improve the crystalline quality of InGaN active regions and reduce QCSE. Another issue is the hue of the InGaN QWs emission: it is determined by the spectral width. This is a key obstacle to realize pure red emissions. Also, the hue of the emission changes with different current densities, which influences the color stability of InGaN-based red LEDs. In contrast, GaN:Eu red LEDs have remarkable emission stability.

From the prospective view, III-nitride red LEDs are a very attractive material to develop full-color μLED displays by monolithically integrated RGB colors. This can lead to high EQE and temperature stability compared to that of AlGaInP systems especially when the device dimensions shrink. The great potential of III-nitride materials can lead to practical GaN-based optoelectronic devices for display applications.

Data availability statement

All data that support the findings of this study are included within the article (and any supplementary files).

Acknowledgment

Some results used in this paper were financially supported by King Abdullah University of Science and Technology (KAUST) (BAS/1/1676-01-01).

ORCID iDs

Daisuke Iida https://orcid.org/0000-0002-5385-6238
Kazuhiro Ohkawa https://orcid.org/0000-0002-8728-3503

References

[1] Araki T, Saito Y, Yamaguchi T, Kurouchi M, Nanishi Y and Naol H 2004 Radio frequency-molecular beam epitaxial growth of InN epitaxial films on (0001) sapphire and their properties *J. Vac. Sci. Technol.* B **22** 2139–43
[2] Brunner D, Angerer H, Bustarret E, Freudenberg F, Höpler R, Dimitrov R, Ambacher O and Stutzmann M 1997 Optical constants of epitaxial AlGaN films and their temperature dependence *J. Appl. Phys.* **82** 5090–6
[3] Hurni C A *et al* 2015 Bulk GaN flip-chip violet light-emitting diodes with optimized efficiency for high-power operation *Appl. Phys. Lett.* **106** 031101
[4] Narukawa Y, Ichikawa M, Sanga D, Sano M and Mukai T 2010 White light emitting diodes with super-high luminous efficacy *J. Phys. D: Appl. Phys.* **43** 354002
[5] Houser K W, Wei M, David A and Krames M R 2014 Whiteness perception under LED illumination *Leukos* **10** 165–80
[6] Schubert E F and Kim J K 2005 Solid-state light sources getting smart *Science* **308** 1274
[7] Narukawa Y, Niki I, Izuno K, Yamada M, Murazaki Y and Mukai T 2002 Phosphor-conversion white light emitting diode using InGaN near-ultraviolet chip *Jpn. J. Appl. Phys.* **41** L371–3
[8] Hsiang E-L, Yang Z, Yang Q, Lan Y-F and Wu S-T 2021 Prospects and challenges of mini-LED, OLED, and micro-LED displays *J. Soc. Inf. Disp.* **29** 446–65
[9] Bi Z, Chen Z, Danesh F and Samuelson L 2021 From nanoLEDs to the realization of RGB-emitting microLEDs *Semicond. Semimet.* **106** 223–51
[10] Broell M, Sundgren P, Rudolph A, Schmid W, Vogl A and Behringer M 2014 New developments on high-efficiency infrared and InGaAlP light-emitting diodes at OSRAM opto semiconductors *Proc. SPIE* **9003** 90030L
[11] Jiang F, Hyun B-R, Zhang Y and Liu Z 2021 Role of intrinsic surface states in efficiency attenuation of GaN-based micro-light-emitting-diodes *Phys. Status Solidi* **15** 2000487
[12] Lee J-M, Huh C, Kim D-J and Park S-J 2003 Dry-etch damage and its recovery in InGaN/GaN multi-quantum-well light-emitting diodes *Semicond. Sci. Technol.* **18** 530–4
[13] Olivier F, Tirano S, Dupré L, Aventurier B, Largeron C and Templier F 2017 Influence of size-reduction on the performances of GaN-based micro-LEDs for display application *J. Lumin.* **191** 112–6
[14] Olivier F, Daami A, Licitra C and Templier F 2017 Shockley-Read-Hall and Auger non-radiative recombination in GaN based LEDs: a size effect study *Appl. Phys. Lett.* **111** 022104
[15] Bulashevich K A and Karpov S Y 2016 Impact of surface recombination on efficiency of III-nitride light-emitting diodes *Phys. Status Solidi* **10** 480–4

[16] Oh J-T *et al* 2018 Light output performance of red AlGaInP-based light emitting diodes with different chip geometries and structures *Opt. Express* **26** 11194–200

[17] Boroditsky M, Gontijo I, Jackson M, Vrijen R, Yablonovitch E, Krauss T, Cheng C-C, Scherer A, Bhat R and Krames M 2000 Surface recombination measurements on III–V candidate materials for nanostructure light-emitting diodes *J. Appl. Phys.* **87** 3497–504

[18] Zhao Y *et al* 2021 2000 PPI silicon-based AlGaInP red micro-LED arrays fabricated via wafer bonding and epilayer lift-off *Opt. Express* **29** 20217–28

[19] Wong M S, Hwang D, Alhassan A I, Lee C, Ley R, Nakamura S and DenBaars S P 2018 High efficiency of III-nitride micro-light-emitting diodes by sidewall passivation using atomic layer deposition *Opt. Express* **26** 21324–31

[20] Jiang X, Zheng C, Mo C, Wang X, Zhang J, Quan Z, Liu J and Jiang F 2019 Study on the performance of InGaN-based green LED by designing different preparing layers *Opt. Mater.* **89** 505–11

[21] Lv Q, Liu J, Mo C, Zhang J, Wu X, Wu Q and Jiang F 2019 Realization of highly efficient InGaN green LEDs with sandwich-like multiple quantum well structure: role of enhanced interwell carrier transport *ACS Photonics* **6** 130–8

[22] Li P P *et al* 2018 Very high external quantum efficiency and wall-plug efficiency 527 nm InGaN green LEDs by MOCVD *Opt. Express* **26** 33108–15

[23] Ichikawa S, Shiomi K, Morikawa T, Timmerman D, Sasaki Y, Tatebayashi J and Fujiwara Y 2021 Eu-doped GaN and InGaN monolithically stacked full-color LEDs with a wide color gamut *Appl. Phys. Express* **14** 031008

[24] Zhuang Z, Iida D and Ohkawa K 2021 Investigation of InGaN-based red/green micro-light-emitting diodes *Opt. Lett.* **46** 1912–5

[25] Robin Y, Pristovsek M, Amano H, Oehler F, Oliver R A and Humphreys C J 2018 What is red? On the chromaticity of orange-red InGaN/GaN based LEDs *J. Appl. Phys.* **124** 183102

[26] Takeuchi T, Sota S, Katsuragawa M, Komori M, Takeuchi H, Amano H and Akasaki I 1997 Quantum-confined Stark effect due to piezoelectric fields in GaInN strained quantum wells *Jpn. J. Appl. Phys.* **36** L382–5

[27] Takeuchi T, Wetzel C, Yamaguchi S, Sakai H, Amano H, Akasaki I, Kaneko Y, Nakagawa S, Yamaoka Y and Yamada N 1998 Determination of piezoelectric fields in strained GaInN quantum wells using the quantum-confined Stark effect *Appl. Phys. Lett.* **73** 1691–3

[28] Mukai T, Yamada M and Nakamura S 1999 Characteristics of InGaN-based UV/blue/green/amber/red light-emitting diodes *Jpn. J. Appl. Phys.* **38** 3976–81

[29] Hwang J-I, Hashimoto R, Saito S and Nunoue S 2014 Development of InGaN-based red LED grown on (0001) polar surface *Appl. Phys. Express* **7** 071003

[30] Koukitu A, Takahashi N, Taki T and Seki H 1997 Thermodynamic analysis of the MOVPE growth of $In_xGa_{1-x}N$ *J. Cryst. Growth* **170** 306–11

[31] Yamashita Y, Tamura H, Horio N, Sato H, Taniguchi K, Chinone T, Omori S and Funaoka C 2003 Control of emission wavelength of GaInN single quantum well, light emitting diodes grown by metalorganic chemical vapor deposition in a split-flow reactor *Jpn. J. Appl. Phys.* **42** 4197–202

[32] Shimizu M, Kawaguchi Y, Hiramatsu K and Sawaki N 1997 Metalorganic vapor phase epitaxy of thick InGaN on sapphire substrate *Jpn. J. Appl. Phys.* **36** 3381–4

[33] Holec D, Costa P M F J, Kappers M J and Humphreys C J 2007 Critical thickness calculations for InGaN/GaN *J. Cryst. Growth* **303** 314–7

[34] Iida D, Zhuang Z, Kirilenko P, Velazquez-Rizo M and Ohkawa K 2020 Demonstration of low forward voltage InGaN-based red LEDs *Appl. Phys. Express* **13** 031001

[35] Iida D, Zhuang Z, Kirilenko P, Velazquez-Rizo M, Najmi M A and Ohkawa K 2020 633-nm InGaN-based red LEDs grown on thick underlying GaN layers with reduced in-plane residual stress *Appl. Phys. Lett.* **116** 162101

[36] Zhang S *et al* 2020 Efficient emission of InGaN-based light-emitting diodes: toward orange and red *Photon. Res.* **8** 1671–5

[37] I-hsiu Ho G B S 1996 Solid phase immiscibility in GaInN *Appl. Phys. Lett.* **69** 2701–3

[38] Ohkawa K, Ichinohe F, Watanabe T, Nakamura K and Iida D 2019 Metalorganic vapor-phase epitaxial growth simulation to realize high-quality and high-In-content InGaN alloys *J. Cryst. Growth* **512** 69–73

[39] MacChesney J B, Bridenbaugh P M and O'Connor P B 1970 Thermal stability of indium nitride at elevated temperatures and nitrogen pressures *Mater. Res. Bull.* **5** 783–91

[40] Belyaev K G, Rakhlin M V, Jmerik V N, Mizerov A M, Kuznetsova Y V, Zamoryanskaya M V, Ivanov S V and Toropov A A 2013 Phase separation in $In_xGa_{1-x}N$ ($0.10 < x < 0.40$) *Phys. Status Solidi* c **10** 527–31

[41] Müller M, Smith G D W, Gault B and Grovenor C R M 2012 Phase separation in thick InGaN layers—a quantitative, nanoscale study by pulsed laser atom probe tomography *Acta Mater.* **60** 4277–85

[42] Oliver R A, Kappers M J, Humphreys C J and Briggs G A D 2005 Growth modes in heteroepitaxy of InGaN on GaN *J. Appl. Phys.* **97** 013707

[43] Koleske D D, Lee S R, Crawford M H, Cross K C, Coltrin M E and Kempisty J M 2014 Connection between GaN and InGaN growth mechanisms and surface morphology *J. Cryst. Growth* **391** 85–96

[44] Pantha B N, Wang H, Khan N, Lin J Y and Jiang H X 2011 Origin of background electron concentration in $In_xGa_{1-x}N$ alloys *Phys. Rev.* B **84** 075327

[45] Pantha B N, Li J, Lin J Y and Jiang H X 2008 Single phase $In_xGa_{1-x}N$ ($0.25 \leqslant x \leqslant 0.63$) alloys synthesized by metal organic chemical vapor deposition *Appl. Phys. Lett.* **93** 182107

[46] Ishikawa M, Ohba Y, Sugawara H, Yamamoto M and Nakanisi T 1986 Room-temperature cw operation of InGaP/InGaAlP visible light laser diodes on GaAs substrates grown by metalorganic chemical vapor deposition *Appl. Phys. Lett.* **48** 207–8

[47] Ikeda M, Mori Y, Takiguchi M, Kaneko K and Watanabe N 1984 cw operation of an AlGaInP double heterostructure laser diode at 77 K grown by atmospheric metalorganic chemical vapor deposition *Appl. Phys. Lett.* **45** 661–3

[48] Van't Blik H, Boerrigter-Lammers J, Valster A and Acket G 1989 Index-guided GaAs/AlGaAs quantum well lasers grown by MOVPE *Proc. SPIE* **1025** 48–51

[49] Kangawa Y, Ito T, Mori A and Koukitu A 2000 Anomalous behavior of excess energy curves of $In_xGa_{1-x}N$ grown on GaN and InN *J. Cryst. Growth* **220** 401–4

[50] Ohkawa K 2020 Simulation of nitride semiconductor MOVPE *Digital Encyclopedia of Applied Physics* (Wiley-VCH) pp 1–20

[51] Kangawa Y, Akiyama T, Ito T, Shiraishi K and Nakayama T 2013 Surface stability and growth kinetics of compound semiconductors: an *ab initio*-based approach *Materials* **6** 3309–60

[52] Kusaba A, Kangawa Y, Honda Y, Amano H and Kakimoto K 2016 Theoretical approach to surface reconstruction of InN(0001) during raised-pressure metalorganic vapor-phase epitaxy *Jpn. J. Appl. Phys.* **55** 05FM01

[53] Matsuoka T, Liu Y, Kimura T, Zhang Y, Prasertsuk K and Katayama R 2011 Paving the way to high-quality indium nitride: the effects of pressurized reactor *Proc. SPIE* **7945** 794519

[54] Senevirathna M K I *et al* 2012 Effect of reactor pressure on the electrical and structural properties of InN epilayers grown by high-pressure chemical vapor deposition *J. Vac. Sci. Technol.* A **30** 031511

[55] Iida D, Nagata K, Makino T, Iwaya M, Kamiyama S, Amano H, Akasaki I, Bandoh A and Udagawa T 2010 Growth of GaInN by raised-pressure metalorganic vapor phase epitaxy *Appl. Phys. Express* **3** 075601

[56] Ohkawa K, Watanabe T, Sakamoto M, Hirako A and Deura M 2012 740-nm emission from InGaN-based LEDs on *c*-plane sapphire substrates by MOVPE *J. Cryst. Growth* **343** 13–16

[57] Hashimoto R, Hwang J, Saito S and Nunoue S 2013 High-efficiency green-yellow light-emitting diodes grown on sapphire (0001) substrates *Phys. Status Solidi* c **10** 1529–32

[58] Alhassan A I, Young N G, Farrell R M, Pynn C, Wu F, Alyamani A Y, Nakamura S, DenBaars S P and Speck J S 2018 Development of high performance green *c*-plane III-nitride light-emitting diodes *Opt. Express* **26** 5591–601

[59] Rhode S L, Fu W Y, Moram M A, Massabuau F C P, Kappers M J, McAleese C, Oehler F, Humphreys C J, Dusane R O and Sahonta S L 2014 Structure and strain relaxation effects of defects in $In_xGa_{1-x}N$ epilayers *J. Appl. Phys.* **116** 103513

[60] Smalc-Koziorowska J, Grzanka E, Czernecki R, Schiavon D and Leszczyński M 2015 Elimination of trench defects and V-pits from InGaN/GaN structures *Appl. Phys. Lett.* **106** 101905

[61] El Gmili Y, Orsal G, Pantzas K, Moudakir T, Sundaram S, Patriarche G, Hester J, Ahaitouf A, Salvestrini J P and Ougazzaden A 2013 Multilayered InGaN/GaN structure vs. single InGaN layer for solar cell applications: a comparative study *Acta Mater.* **61** 6587–96

[62] Srinivasan S, Geng L, Liu R, Ponce F A, Narukawa Y and Tanaka S 2003 Slip systems and misfit dislocations in InGaN epilayers *Appl. Phys. Lett.* **83** 5187–9

[63] Hiramatsu K, Kawaguchi Y, Shimizu M, Sawaki N, Zheleva T, Davis R F, Tsuda H, Taki W, Kuwano N and Oki K 1997 The composition pulling effect in MOVPE grown InGaN on GaN and AlGaN and its TEM characterization *MRS Int. J. Nitride Semicond. Res.* **2** 11

[64] Mizuseki H, Gueriba J S, Empizo M J F, Sarukura N, Kawazoe Y and Ohkawa K 2021 Atomistic origin of compositional pulling effect in wurtzite (B, Al, In)$_x$Ga$_{1-x}$N: a first-principles study *J. Appl. Phys.* **130** 035704

[65] Senda R, Matsubara T, Iida D, Iwaya M, Kamiyama S, Amano H and Akasaki I 2009 Strong emission from GaInN/GaN multiple quantum wells on high-crystalline-quality thick *m*-plane GaInN underlying layer on grooved GaN *Appl. Phys. Express* **2** 061004

[66] Koslow I L, McTaggart C, Wu F, Nakamura S, Speck J S and DenBaars S P 2014 Improved performance of (20–21) long-wavelength light-emitting diodes grown with wide quantum wells on stress-relaxed $In_xGa_{1-x}N$ buffer layers *Appl. Phys. Express* **7** 031003

[67] Pantzas K *et al* 2013 Semibulk InGaN: a novel approach for thick, single phase, epitaxial InGaN layers grown by MOVPE *J. Cryst. Growth* **370** 57–62

[68] Eldred T B, Abdelhamid M, Reynolds J G, El-Masry N A, LeBeau J M and Bedair S M 2020 Observing relaxation in device quality InGaN templates by TEM techniques *Appl. Phys. Lett.* **116** 102104

[69] Däubler J, Passow T, Aidam R, Köhler K, Kirste L, Kunzer M and Wagner J 2014 Long wavelength emitting GaInN quantum wells on metamorphic GaInN buffer layers with enlarged in-plane lattice parameter *Appl. Phys. Lett.* **105** 111111

[70] Pasayat S S, Gupta C, Acker-James D, Cohen D A, DenBaars S P, Nakamura S, Keller S and Mishra U K 2019 Fabrication of relaxed InGaN pseudo-substrates composed of micron-sized pattern arrays with high fill factors using porous GaN *Semicond. Sci. Technol.* **34** 115020

[71] Pasayat S S, Gupta C, Wang Y, DenBaars S P, Nakamura S, Keller S and Mishra U K 2020 Compliant micron-sized patterned InGaN pseudo-substrates utilizing porous GaN *Materials* **13** 213

[72] Pasayat S S, Gupta C, Wong M S, Wang Y, Nakamura S, Denbaars S P, Keller S and Mishra U K 2020 Growth of strain-relaxed InGaN on micrometer-sized patterned compliant GaN pseudo-substrates *Appl. Phys. Lett.* **116** 111101

[73] Pasayat S S, Hatui N, Li W, Gupta C, Nakamura S, Denbaars S P, Keller S and Mishra U K 2020 Method of growing elastically relaxed crack-free AlGaN on GaN as substrates for ultra-wide bandgap devices using porous GaN *Appl. Phys. Lett.* **117** 062102

[74] Pasayat S S, Gupta C, Wong M S, Ley R, Gordon M J, DenBaars S P, Nakamura S, Keller S and Mishra U K 2021 Demonstration of ultra-small (<10 μm) 632 nm red InGaN micro-LEDs with useful on-wafer external quantum efficiency (>0.2%) for mini-displays *Appl. Phys. Express* **14** 011004

[75] Even A, Laval G, Ledoux O, Ferret P, Sotta D, Guiot E, Levy F, Robin I C and Dussaigne A 2017 Enhanced In incorporation in full InGaN heterostructure grown on relaxed InGaN pseudo-substrate *Appl. Phys. Lett.* **110** 262103

[76] Cooper D, Boureau V, Even A, Barbier F and Dussaigne A 2020 Determination of the internal piezoelectric potentials and indium concentration in InGaN based quantum wells grown on relaxed InGaN pseudo-substrates by off-axis electron holography *Nanotechnology* **31** 475705

[77] Dussaigne A *et al* 2020 Full InGaN red light emitting diodes *J. Appl. Phys.* **128** 135704

[78] Dussaigne A, Barbier F, Samuel B, Even A, Templier R, Lévy F, Ledoux O, Rozhavskaia M and Sotta D 2020 Strongly reduced V pit density on InGaNOS substrate by using InGaN/GaN superlattice *J. Cryst. Growth* **533** 125481

[79] Samuel B, Cooper D, Rochat N, Mavel A, Barbier F and Dussaigne A 2021 Origins of nanoscale emission inhomogeneities of high content red emitting InGaN/InGaN quantum wells *J. Appl. Phys.* **129** 173105

[80] Kobayashi A, Ohta J and Fujioka H 2006 Low temperature epitaxial growth of $In_{0.25}Ga_{0.75}N$ on lattice-matched ZnO by pulsed laser deposition *J. Appl. Phys.* **99** 123513

[81] Shimomoto K, Kobayashi A, Ueno K, Ohta J, Oshima M, Fujioka H, Amanai H, Nagao S and Horie H 2009 Room-temperature epitaxial growth of high-quality *m*-plane InGaN films on ZnO substrates *Phys. Status Solidi* **3** 124–6

[82] Kobayashi A, Ohta J and Fujioka H 2006 Characteristics of InGaN with high in concentrations grown on ZnO at low temperatures *Jpn. J. Appl. Phys.* **45** L611–3

[83] Kobayashi A, Ohta J and Fujioka H 2017 Pulsed sputtering epitaxial growth of *m*-plane InGaN lattice-matched to ZnO *Sci. Rep.* **7** 12820

[84] Yu H, Wang S, Li N, Fenwick W, Melton A, Klein B and Ferguson I 2008 MOVPE growth of AlGaN/GaN superlattices on ZnO substrates for green emitter applications *J. Cryst. Growth* **310** 4904–7

[85] Hellman E S, Buchanan D N E, Wiesmann D and Brener I 1996 Growth of Ga-face and N-face GaN films using ZnO substrates *MRS Int. J. Nitride Semicond. Res.* **1** U117–23

[86] Hong S-K, Hanada T, Ko H-J, Chen Y, Yao T, Imai D, Araki K and Shinohara M 2000 Control of polarity of ZnO films grown by plasma-assisted molecular-beam epitaxy: Zn- and O-polar ZnO films on Ga-polar GaN templates *Appl. Phys. Lett.* **77** 3571–3

[87] Xia Y *et al* 2013 Blue light-emitting diodes grown on ZnO substrates *Appl. Phys. Express* **6** 042101

[88] Wang S-J, Li N, Park E-H, Feng Z C, Valencia A, Nause J, Kane M, Summers C and Ferguson I 2008 MOCVD growth of GaN-based materials on ZnO substrates *Phys. Status Solidi* c **5** 1736–9

[89] Lei Y, Xu J, Zhu K, He M, Zhou J, Gao Y, Zhang L and Chen Y 2013 A GaN-based LED with perpendicular structure fabricated on a ZnO substrate by MOCVD *J. Disp. Technol.* **9** 377–81

[90] Ueta A, Ohno H, Yanagita N, Ryoki N, Miyano K, Ishibashi A and Nobuoka M 2019 High quality nitride semiconductors grown on novel $ScAlMgO_4$ substrates and their light emitting diodes *Jpn. J. Appl. Phys.* **58** SC1041

[91] Ozaki T, Funato M and Kawakami Y 2015 InGaN-based visible light-emitting diodes on $ScAlMgO_4$(0001) substrates *Appl. Phys. Express* **8** 062101

[92] Ozaki T, Takagi Y, Nishinaka J, Funato M and Kawakami Y 2014 Metalorganic vapor phase epitaxy of GaN and lattice-matched InGaN on $ScAlMgO_4$(0001) substrates *Appl. Phys. Express* **7** 091001

[93] Ozaki T, Funato M and Kawakami Y 2019 Red-emitting $In_xGa_{1-x}N/In_yGa_{1-y}N$ quantum wells grown on lattice-matched $In_yGa_{1-y}N/ScAlMgO_4$(0001) templates *Appl. Phys. Express* **12** 011007

[94] Liu L and Edgar J H 2002 Substrates for gallium nitride epitaxy *Mater. Sci. Eng.* R **37** 61–127

[95] Stanimirovic A, Balzaretti N M, Feldman A and Graebner J E 2001 Thermal conductivity and thermal diffusivity of selected oxide single crystals *J. Mater. Res.* **16** 678–82

[96] Alam S, Sundaram S, Li X, El Gmili Y, Elouneg-Jamroz M, Robin I C, Patriarche G, Salvestrini J-P, Voss P L and Ougazzaden A 2017 Emission wavelength red-shift by using 'semi-bulk' InGaN buffer layer in InGaN/InGaN multiple-quantum-well *Superlattices Microstruct.* **112** 279–86

[97] Abdelhamid M, Routh E L and Bedair S M 2021 The dependence of the emission from MQWs on the indium content in the underlying InGaN templates: experimental and modeling results *Semicond. Sci. Technol.* **36** 035018

[98] Röder C, Lipski F, Habel F, Leibiger G, Abendroth M, Himcinschi C and Kortus J 2013 Raman spectroscopic characterization of epitaxially grown GaN on sapphire *J. Phys. D: Appl. Phys.* **46** 285302

[99] Johnson M C, Bourret-Courchesne E D, Wu J, Liliental-Weber Z, Zakharov D N, Jorgenson R J, Ng T B, McCready D E and Williams J R 2004 Effect of gallium nitride template layer strain on the growth of $In_xGa_{1-x}N$ /GaN multiple quantum well light emitting diodes *J. Appl. Phys.* **96** 1381–6

[100] Hiramatsu K, Detchprohm T and Akasaki I 1993 Relaxation mechanism of thermal stresses in the heterostructure of GaN grown on sapphire by vapor phase epitaxy *Jpn. J. Appl. Phys.* **32** 1528–33

[101] Muhammed M M, Roldan M A, Yamashita Y, Sahonta S L, Ajia I A, Iizuka K, Kuramata A, Humphreys C J and Roqan I S 2016 High-quality III-nitride films on conductive, transparent (201)-oriented beta-Ga_2O_3 using a GaN buffer layer *Sci. Rep.* **6** 29747

[102] Qi W *et al* 2017 Effects of thickness ratio of InGaN to GaN in superlattice strain relief layer on the optoelectrical properties of InGaN-based green LEDs grown on Si substrates *J. Appl. Phys.* **122** 084504

[103] Tao X *et al* 2018 Performance enhancement of yellow InGaN-based multiple-quantum-well light-emitting diodes grown on Si substrates by optimizing the InGaN/GaN superlattice interlayer *Opt. Mater. Express* **8** 1221

[104] Jiang F *et al* 2019 Efficient InGaN-based yellow-light-emitting diodes *Photon. Res.* **7** 141–8

[105] Zhang J, Xiong C, Liu J, Quan Z, Wang L and Jiang F 2014 High brightness InGaN-based yellow light-emitting diodes with strain modulation layers grown on Si substrate *Appl. Phys.* A **114** 1049–53

[106] Haller C, Carlin J F, Jacopin G, Martin D, Butté R and Grandjean N 2017 Burying non-radiative defects in InGaN underlayer to increase InGaN/GaN quantum well efficiency *Appl. Phys. Lett.* **111** 262101

[107] Haller C, Carlin J F, Jacopin G, Liu W, Martin D, Butté R and Grandjean N 2018 GaN surface as the source of non-radiative defects in InGaN/GaN quantum wells *Appl. Phys. Lett.* **113** 111106

[108] Akasaka T, Gotoh H, Saito T and Makimoto T 2004 High luminescent efficiency of InGaN multiple quantum wells grown on InGaN underlying layers *Appl. Phys. Lett.* **85** 3089–91

[109] Akasaka T, Gotoh H, Kobayashi Y, Nakano H and Makimoto T 2006 InGaN quantum wells with small potential fluctuation grown on InGaN underlying layers *Appl. Phys. Lett.* **89** 101110

[110] Hangleiter A, Hitzel F, Netzel C, Fuhrmann D, Rossow U, Ade G and Hinze P 2005 Suppression of nonradiative recombination by V-shaped pits in GaInN/GaN quantum wells produces a large increase in the light emission efficiency *Phys. Rev. Lett.* **95** 127402

[111] Kim J, Cho Y H, Ko D S, Li X S, Won J Y, Lee E, Park S H, Kim J Y and Kim S 2014 Influence of V-pits on the efficiency droop in InGaN/GaN quantum wells *Opt. Express* **22** A857–66

[112] Netzel C, Bremers H, Hoffmann L, Fuhrmann D, Rossow U and Hangleiter A 2007 Emission and recombination characteristics of $Ga_{1-x}In_xN$/GaN quantum well structures with nonradiative recombination suppression by V-shaped pits *Phys. Rev.* B **76** 155322

[113] Chang C-Y, Li H, Shih Y-T and Lu T-C 2015 Manipulation of nanoscale V-pits to optimize internal quantum efficiency of InGaN multiple quantum wells *Appl. Phys. Lett.* **106** 091104

[114] Wu X, Liu J and Jiang F 2015 Hole injection from the sidewall of V-shaped pits into *c*-plane multiple quantum wells in InGaN light emitting diodes *J. Appl. Phys.* **118** 164504

[115] Li C-K, Wu C-K, Hsu C-C, Lu L-S, Li H, Lu T-C and Wu Y-R 2016 3D numerical modeling of the carrier transport and radiative efficiency for InGaN/GaN light emitting diodes with V-shaped pits *AIP Adv.* **6** 055208

[116] Kang D, Oh J-T, Song J-O, Seong T-Y, Kneissl M and Amano H 2019 Hole injection mechanism in the quantum wells of blue light emitting diode with V pits for micro-display application *Appl. Phys. Express* **12** 102016

[117] Iida D, Niwa K, Kamiyama S and Ohkawa K 2016 Demonstration of InGaN-based orange LEDs with hybrid multiple-quantum-wells structure *Appl. Phys. Express* **9** 111003

[118] Yoshida H, Hikosaka T, Nago H and Nunoue S 2015 Impact of dislocations and defects on the relaxation behavior of

InGaN/GaN multiple quantum wells grown on Si and sapphire substrates *Phys. Status Solidi* b **252** 917–22
[119] Meng Y, Wang L, Li F, Zhao G, Yao W, Yang S and Wang Z 2019 Growth and characterization of amber light-emitting diodes with dual-wavelength InGaN/GaN multiple-quantum-well structures *Mater. Res. Express* **6** 0850c8
[120] Yao W, Wang L, Meng Y, Yang S, Liu X, Niu H and Wang Z 2021 Stress engineering for reducing the injection current induced blue shift in InGaN-based red light-emitting diodes *CrystEngComm* **23** 2360–6
[121] Iida D, Lu S, Hirahara S, Niwa K, Kamiyama S and Ohkawa K 2016 Enhanced light output power of InGaN-based amber LEDs by strain-compensating AlN/AlGaN barriers *J. Cryst. Growth* **448** 105–8
[122] Koleske D D, Fischer A J, Bryant B N, Kotula P G and Wierer J J 2015 On the increased efficiency in InGaN-based multiple quantum wells emitting at 530–590 nm with AlGaN interlayers *J. Cryst. Growth* **415** 57–64
[123] Doi T, Honda Y, Yamaguchi M and Amano H 2013 Strain-compensated effect on the growth of InGaN/AlGaN multi-quantum well by metalorganic vapor phase epitaxy *Jpn. J. Appl. Phys.* **52** 08JB14
[124] Lekhal K, Damilano B, Ngo H T, Rosales D, de Mierry P, Hussain S, Vennéguès P and Gil B 2015 Strain-compensated (Ga,In)N/(Al,Ga)N/GaN multiple quantum wells for improved yellow/amber light emission *Appl. Phys. Lett.* **106** 142101
[125] Keller S, Fichtenbaum N A, Furukawa M, Speck J S, DenBaars S P and Mishra U K 2007 Growth and characterization of N-polar InGaN/GaN multiquantum wells *Appl. Phys. Lett.* **90** 191908
[126] Nath D N, Gür E, Ringel S A and Rajan S 2010 Molecular beam epitaxy of N-polar InGaN *Appl. Phys. Lett.* **97** 071903
[127] Wernicke T, Schade L, Netzel C, Rass J, Hoffmann V, Ploch S, Knauer A, Weyers M, Schwarz U and Kneissl M 2012 Indium incorporation and emission wavelength of polar, nonpolar and semipolar InGaN quantum wells *Semicond. Sci. Technol.* **27** 024014
[128] Shojiki K, Tanikawa T, Choi J-H, Kuboya S, Hanada T, Katayama R and Matsuoka T 2015 Red to blue wavelength emission of N-polar (000–1) InGaN light-emitting diodes grown by metalorganic vapor phase epitaxy *Appl. Phys. Express* **8** 061005
[129] Wang Y, Shimma R, Yamamoto T, Hayashi H, Shiohama K-I, Kurihara K, Hasegawa R and Ohkawa K 2015 The effect of plane orientation on indium incorporation into InGaN/GaN quantum wells fabricated by MOVPE *J. Cryst. Growth* **416** 164–8
[130] Akyol F, Nath D N, Gür E, Park P S and Rajan S 2011 N-polar III–nitride green (540 nm) light emitting diode *Jpn. J. Appl. Phys.* **50** 052101
[131] Akyol F, Nath D N, Krishnamoorthy S, Park P S and Rajan S 2012 Suppression of electron overflow and efficiency droop in N-polar GaN green light emitting diodes *Appl. Phys. Lett.* **100** 111118
[132] Funato M, Ueda M, Kawakami Y, Narukawa Y, Kosugi T, Takahashi M and Mukai T 2006 Blue, green, and amber InGaN/GaN light-emitting diodes on semipolar {11-22} GaN bulk substrates *Jpn. J. Appl. Phys.* **45** L659–62
[133] Bai J, Xu B, Guzman F G, Xing K, Gong Y, Hou Y and Wang T 2015 (11–22) semipolar InGaN emitters from green to amber on overgrown GaN on micro-rod templates *Appl. Phys. Lett.* **107** 261103
[134] Zhao Y, Fu H, Wang G T and Nakamura S 2018 Toward ultimate efficiency: progress and prospects on planar and 3D nanostructured nonpolar and semipolar InGaN light-emitting diodes *Adv. Opt. Photon.* **10** 246
[135] Shojiki K, Hanada T, Tanikawa T, Imai Y, Kimura S, Nonoda R, Kuboya S, Katayama R and Matsuoka T 2016 Homogeneity improvement of N-polar (000–1) InGaN/GaN multiple quantum wells by using *c*-plane sapphire substrate with off-cut-angle toward a-sapphire plane *Jpn. J. Appl. Phys.* **55** 05FA09
[136] Tanikawa T, Shojiki K, Aisaka T, Kimura T, Kuboya S, Hanada T, Katayama R and Matsuoka T 2014 Enhancement of surface migration by Mg doping in the metalorganic vapor phase epitaxy of N-polar (000–1) GaN/sapphire *Jpn. J. Appl. Phys.* **53** 05FL05
[137] Keller S, Fichtenbaum N A, Wu F, Brown D, Rosales A, DenBaars S P, Speck J S and Mishra U K 2007 Influence of the substrate misorientation on the properties of N-polar GaN films grown by metal organic chemical vapor deposition *J. Appl. Phys.* **102** 083546
[138] Tanikawa T, Kuboya S and Matsuoka T 2017 Control of impurity concentration in N-polar (000–1) GaN grown by metalorganic vapor phase epitaxy *Phys. Status Solidi* b **254** 1600751
[139] Lund C, Nakamura S, DenBaars S P, Mishra U K and Keller S 2019 Properties of N-polar InGaN/GaN quantum wells grown with triethyl gallium and triethyl indium as precursors *Semicond. Sci. Technol.* **34** 075017
[140] Li C, Zhang K, Qiaoyu Z, Yin X, Ge X, Wang J, Wang Q, He C, Zhao W and Chen Z 2020 High quality N-polar GaN films grown with varied V/III ratios by metal–organic vapor phase epitaxy *RSC Adv.* **10** 43187–92
[141] Lund C *et al* 2017 Metal-organic chemical vapor deposition of high quality, high indium composition N-polar InGaN layers for tunnel devices *J. Appl. Phys.* **121** 185707
[142] Aisaka T, Tanikawa T, Kimura T, Shojiki K, Hanada T, Katayama R and Matsuoka T 2014 Improvement of surface morphology of nitrogen-polar GaN by introducing indium surfactant during MOVPE growth *Jpn. J. Appl. Phys.* **53** 085501
[143] Hatui N, Krishna A, Pasayat S S, Keller S and Mishra U K 2021 Metal organic vapor phase epitaxy of thick N-polar InGaN films *Electronics* **10** 1182
[144] Cruz S C, Keller S, Mates T E, Mishra U K and DenBaars S P 2009 Crystallographic orientation dependence of dopant and impurity incorporation in GaN films grown by metalorganic chemical vapor deposition *J. Cryst. Growth* **311** 3817–23
[145] Browne D A, Young E C, Lang J R, Hurni C A and Speck J S 2012 Indium and impurity incorporation in InGaN films on polar, nonpolar, and semipolar GaN orientations grown by ammonia molecular beam epitaxy *J. Vac. Sci. Technol.* A **30** 041513
[146] Dreyer C E, Alkauskas A, Lyons J L, Speck J S and Walle C G V D 2016 Gallium vacancy complexes as a cause of Shockley-Read-Hall recombination in III-nitride light emitters *Appl. Phys. Lett.* **108** 141101
[147] Ueno K, Kishikawa E, Ohta J and Fujioka H 2017 N-polar InGaN-based LEDs fabricated on sapphire via pulsed sputtering *APL Mater.* **5** 026102
[148] Seo Y G, Baik K H, Song H, Son J-S, Oh K and Hwang S-M 2011 Orange *a*-plane InGaN/GaN light-emitting diodes grown on *r*-plane sapphire substrates *Opt. Express* **19** 12919–24
[149] Kawaguchi Y, Huang C-Y, Wu Y-R, Zhao Y, DenBaars S P and Nakamura S 2013 Semipolar (2021) single-quantum-well red light-emitting diodes with a low forward voltage *Jpn. J. Appl. Phys.* **52** 08JC08
[150] Khoury M *et al* 2019 Demonstration of electrically injected semipolar laser diodes grown on low-cost and scalable

sapphire substrates *ACS Appl. Mater. Interfaces* **11** 47106–11
[151] Murayama M, Nakayama Y, Yamazaki K, Hoshina Y, Watanabe H, Fuutagawa N, Kawanishi H, Uemura T and Narui H 2018 Watt-class green (530 nm) and blue (465 nm) laser diodes *Phys. Status Solidi* a **215** 1700513
[152] Mehari S, Cohen D A, Becerra D L, Nakamura S and DenBaars S P 2018 Demonstration of enhanced continuous-wave operation of blue laser diodes on a semipolar 20–2–1 GaN substrate using indium-tin-oxide/thin-p-GaN cladding layers *Opt. Express* **26** 1564–72
[153] Hamaguchi T *et al* 2020 Room-temperature continuous-wave operation of green vertical-cavity surface-emitting lasers with a curved mirror fabricated on {20−21} semi-polar GaN *Appl. Phys. Express* **13** 041002
[154] Kikuchi A, Kawai M, Tada M and Kishino K 2004 InGaN/GaN multiple quantum disk nanocolumn light-emitting diodes grown on (111) Si substrate *Jpn. J. Appl. Phys.* **43** L1524–6
[155] Jahangir S, Mandl M, Strassburg M and Bhattacharya P 2013 Molecular beam epitaxial growth and optical properties of red-emitting ($\lambda = 650$ nm) InGaN/GaN disks-in-nanowires on silicon *Appl. Phys. Lett.* **102** 071101
[156] Vadivelu R, Igawa Y and Kishino K 2013 633 nm red emissions from InGaN nanocolumn light-emitting diode by radio frequency plasma assisted molecular beam epitaxy *Jpn. J. Appl. Phys.* **52** 08JE18
[157] Jahangir S, Schimpke T, Strassburg M, Grossklaus K A, Millunchick J M and Bhattacharya P 2014 Red-emitting ($\lambda = 610$ nm) $In_{0.51}Ga_{0.49}N$/GaN disk-in-nanowire light emitting diodes on silicon *IEEE J. Quantum Electron.* **50** 530–7
[158] Zhao C *et al* 2016 Droop-free, reliable, and high-power InGaN/GaN nanowire light-emitting diodes for monolithic metal-optoelectronics *Nano Lett.* **16** 4616–23
[159] Zhao C, Ng T K, Wei N, Prabaswara A, Alias M S, Janjua B, Shen C and Ooi B S 2016 Facile formation of high-quality InGaN/GaN quantum-disks-in-nanowires on bulk-metal substrates for high-power light-emitters *Nano Lett.* **16** 1056–63
[160] Bui H Q T, Velpula R T, Jain B, Aref O H, Nguyen H D, Lenka T R and Nguyen H P T 2019 Full-color InGaN/AlGaN nanowire micro light-emitting diodes grown by molecular beam epitaxy: a promising candidate for next generation micro displays *Micromachines* **10** 492
[161] Yanagihara A and Kishino K 2019 Red-emitting InGaN-based nanocolumn light-emitting diodes with highly directional beam profiles *Phys. Status Solidi* a **217** 1900771
[162] Nguyen H P, Zhang S, Connie A T, Kibria M G, Wang Q, Shih I and Mi Z 2013 Breaking the carrier injection bottleneck of phosphor-free nanowire white light-emitting diodes *Nano Lett.* **13** 5437–42
[163] Ra Y-H, Rashid R T, Liu X, Lee J and Mi Z 2017 Scalable nanowire photonic crystals: molding the light emission of InGaN *Adv. Funct. Mater.* **27** 1702364
[164] Sekiguchi H, Kishino K and Kikuchi A 2010 Emission color control from blue to red with nanocolumn diameter of InGaN/GaN nanocolumn arrays grown on same substrate *Appl. Phys. Lett.* **96** 231104
[165] Kishino K, Sakakibara N, Narita K and Oto T 2020 Two-dimensional multicolor (RGBY) integrated nanocolumn micro-LEDs as a fundamental technology of micro-LED display *Appl. Phys. Express* **13** 014003
[166] Ra Y H, Wang R, Woo S Y, Djavid M, Sadaf S M, Lee J, Botton G A and Mi Z 2016 Full-color single nanowire pixels for projection displays *Nano Lett.* **16** 4608–15
[167] Hong Y J, Lee C H, Yoon A, Kim M, Seong H K, Chung H J, Sone C, Park Y J and Yi G C 2011 Visible-color-tunable light-emitting diodes *Adv. Mater.* **23** 3284–8
[168] Monemar B, Ohlsson B J, Gardner N F and Samuelson L 2016 Nanowire-based visible light emitters, present status and outlook *Semicond. Semimetal.* **94** 227–71
[169] Kum H, Seong H K, Lim W, Chun D, Kim Y I, Park Y and Yoo G 2017 Wafer-scale thermodynamically stable GaN nanorods via two-step self-limiting epitaxy for optoelectronic applications *Sci. Rep.* **7** 40893
[170] Johar M A, Song H-G, Waseem A, Hassan M A, Bagal I V, Cho Y-H and Ryu S-W 2020 Universal and scalable route to fabricate GaN nanowire-based LED on amorphous substrate by MOCVD *Appl. Mater. Today* **19** 100541
[171] Kuykendall T R, Altoe M V, Ogletree D F and Aloni S 2014 Catalyst-directed crystallographic orientation control of GaN nanowire growth *Nano Lett.* **14** 6767–73
[172] Bi Z *et al* 2020 Realization of ultrahigh quality InGaN platelets to be used as relaxed templates for red micro-LEDs *ACS Appl. Mater. Interfaces* **12** 17845–51
[173] Bi Z *et al* 2019 InGaN platelets: synthesis and applications toward green and red light-emitting diodes *Nano Lett.* **19** 2832–9
[174] Ko Y-H, Kim J-H, Gong S-H, Kim J, Kim T and Cho Y-H 2015 Red emission of InGaN/GaN double heterostructures on GaN nanopyramid structures *ACS Photonics* **2** 515–20
[175] Chang S P, Chang J R, Sou K P, Liu M C, Cheng Y J, Kuo H C and Chang C Y 2013 Electrically driven green, olivine, and amber color nanopyramid light emitting diodes *Opt. Express* **21** 23030–5
[176] Jindal V, Tripathi N, Tungare M, Paschos O, Haldar P and Shahedipour-Sandvik F 2008 Selective area heteroepitaxy of low dimensional *a*-plane and *c*-plane InGaN nanostructures using pulsed MOCVD *Phys. Status Solidi* c **5** 1709–11
[177] Song J, Leung B, Zhang Y and Han J 2014 Growth, structural and optical properties of ternary InGaN nanorods prepared by selective-area metalorganic chemical vapor deposition *Nanotechnology* **25** 225602
[178] Sundaram S *et al* 2014 Nanoscale selective area growth of thick, dense, uniform, In-rich, InGaN nanostructure arrays on GaN/sapphire template *J. Appl. Phys.* **116** 163105
[179] Sundaram S, Gmili Y E, Puybaret R, Li X, Bonanno P L, Pantzas K, Patriarche G, Voss P L, Salvestrini J P and Ougazzaden A 2015 Nanoselective area growth and characterization of dislocation-free InGaN nanopyramids on AlN buffered Si(111) templates *Appl. Phys. Lett.* **107** 113105
[180] Bi Z, Gustafsson A, Lenrick F, Lindgren D, Hultin O, Wallenberg L R, Ohlsson B J, Monemar B and Samuelson L 2018 High In-content InGaN nano-pyramids: tuning crystal homogeneity by optimized nucleation of GaN seeds *J. Appl. Phys.* **123** 025102
[181] Schulz S and O'Reilly E P 2010 Theory of reduced built-in polarization field in nitride-based quantum dots *Phys. Rev.* B **82** 033411
[182] Zhao C, Tang C W, Lai B, Cheng G, Wang J and Lau K M 2020 Low-efficiency-droop InGaN quantum dot light-emitting diodes operating in the 'green gap' *Photonics Res.* **8** 750–4
[183] Zhang M, Bhattacharya P and Guo W 2010 InGaN/GaN self-organized quantum dot green light emitting diodes with reduced efficiency droop *Appl. Phys. Lett.* **97** 011103

[184] Meng Y, Wang L, Zhao G, Li F, Li H, Yang S and Wang Z 2018 Red emission of InGaN/GaN multiple-quantum-well light-emitting diode structures with indium-rich clusters *Phys. Status Solidi* a **215** 1800455

[185] Li H, Li P, Kang J, Ding J, Ma J, Zhang Y, Yi X and Wang G 2016 Broadband full-color monolithic InGaN light-emitting diodes by self-assembled InGaN quantum dots *Sci. Rep.* **6** 35217

[186] Wang L *et al* 2021 Green InGaN quantum dots breaking through efficiency and bandwidth bottlenecks of micro-LEDs *Laser Photonics Rev.* **15** 2000406

[187] Soh C B, Liu W, Chua S J, Tan R J N, Ang S S and Chow S Y 2011 Red emitting LEDs formed by indium rich quantum dots incorporated in MQWs *Phys. Status Solidi* a **208** 1579–81

[188] Lv W, Wang L, Wang J, Xing Y, Zheng J, Yang D, Hao Z and Luo Y 2013 Green and red light-emitting diodes based on multilayer InGaN/GaN dots grown by growth interruption method *Jpn. J. Appl. Phys.* **52** 08JG13

[189] Park I-K and Park S-J 2011 Green gap spectral range light-emitting diodes with self-assembled ingan quantum dots formed by enhanced phase separation *Appl. Phys. Express* **4** 042102

[190] Heikenfeld J, Garter M, Lee D S, Birkhahn R and Steckl A J 1999 Red light emission by photoluminescence and electroluminescence from Eu-doped GaN *Appl. Phys. Lett.* **75** 1189–91

[191] Lorenz K, Miranda S M, Alves E, Roqan I, O'Donnell K and Bońkowski M 2012 High pressure annealing of europium implanted GaN *Proc. SPIE* **8262** 82620C

[192] Faye D N *et al* 2016 Study of damage formation and annealing of implanted III-nitride semiconductors for optoelectronic devices *Nucl. Instrum. Methods Phys. Res.* B **379** 251–4

[193] Wang R and Steckl A J 2010 Effect of growth conditions on Eu^{3+} luminescence in GaN *J. Cryst. Growth* **312** 680–4

[194] Hori Y, Enjalbert F, Jalabert D, Monroy E, Dang L S, Biquard X, Tanaka M, Oda O and Daudin B 2003 Visible red light emission from Eu-doped GaN quantum dots grown by plasma-assisted MBE *Phys. Status Solidi* c **0** 2695–8

[195] Andreev T, Liem N Q, Hori Y, Tanaka M, Oda O, Daudin B and Si Dang D L 2006 Comparative optical study of Eu^{3+} ions doping in InGaN/GaN quantum dots and GaN layer grown by molecular beam epitaxy *Opt. Mater.* **28** 775–9

[196] Takagi Y, Suwa T, Sekiguchi H, Okada H and Wakahara A 2011 Effect of Mg codoping on Eu^{3+} luminescence in GaN grown by ammonia molecular beam epitaxy *Appl. Phys. Lett.* **99** 171905

[197] Wakahara A, Sekiguchi H, Okada H and Takagi Y 2012 Current status for light-emitting diode with Eu-doped GaN active layer grown by MBE *J. Lumin.* **132** 3113–7

[198] Sekiguchi H, Takagi Y, Otani T, Okada H and Wakahara A 2013 Emission enhancement mechanism of GaN:Eu by Mg codoping *J. Appl. Phys.* **113** 013105

[199] Sekiguchi H, Sakai M, Kamada T, Yamane K, Okada H and Wakahara A 2019 Observation of single optical site of Eu and Mg codoped GaN grown by NH_3-source molecular beam epitaxy *J. Appl. Phys.* **125** 175702

[200] Sukegawa A, Sekiguchi H, Matsuzaki R, Yamane K, Okada H, Kishino K and Wakahara A 2018 Self-organized Eu-doped GaN nanocolumn light-emitting diode grown by RF-molecular-beam epitaxy *Phys. Status Solidi* a **216** 1800501

[201] Zhu W, Mitchell B, Timmerman D, Koizumi A, Gregorkiewicz T and Fujiwara Y 2017 High-power Eu-doped GaN red LED based on a multilayer structure grown at lower temperatures by organometallic vapor phase epitaxy *MRS Adv.* **2** 159–64

[202] Zhu W, Mitchell B, Timmerman D, Uedono A, Koizumi A and Fujiwara Y 2016 Enhanced photo/electroluminescence properties of Eu-doped GaN through optimization of the growth temperature and Eu related defect environment *APL Mater.* **4** 056103

[203] Mitchell B *et al* 2016 Utilization of native oxygen in Eu(RE)-doped GaN for enabling device compatibility in optoelectronic applications *Sci. Rep.* **6** 18808

[204] Mitchell B, Poplawsky J, Lee D, Koizumi A, Fujiwara Y and Dierolf V 2014 The role of donor-acceptor pairs in the excitation of Eu-ions in GaN:Eu epitaxial layers *J. Appl. Phys.* **115** 204501

[205] Lee D-G, Nishikawa A, Terai Y and Fujiwara Y 2012 Eu luminescence center created by Mg codoping in Eu-doped GaN *Appl. Phys. Lett.* **100** 171904

[206] Nishikawa A, Furukawa N, Kawasaki T, Terai Y and Fujiwara Y 2010 Improved luminescence properties of Eu-doped GaN light-emitting diodes grown by atmospheric-pressure organometallic vapor phase epitaxy *Appl. Phys. Lett.* **97** 051113

[207] Nishikawa A, Kawasaki T, Furukawa N, Terai Y and Fujiwara Y 2009 Room-temperature red emission from a p-type/europium-doped/n-type gallium nitride light-emitting diode under current injection *Appl. Phys. Express* **2** 071004

[208] Lee D-G, Wakamatsu R, Koizumi A, Terai Y and Fujiwara Y 2013 Control of Eu luminescence centers by codoping of Mg and Si into Eu-doped GaN *Jpn. J. Appl. Phys.* **52** 08JM01

[209] Mitchell B, Dierolf V, Gregorkiewicz T and Fujiwara Y 2018 Perspective: toward efficient GaN-based red light emitting diodes using europium doping *J. Appl. Phys.* **123** 160901

[210] Mukai T, Narimatsu H and Nakamura S 1998 Amber InGaN-based light-emitting diodes operable at high ambient temperatures *Jpn. J. Appl. Phys.* **37** L479–81

[211] Mukai T 2002 Recent progress in group-III nitride light-emitting diodes *IEEE J. Sel. Topics Quantum Electron.* **8** 264–70

[212] Chen H-S, Lu C-F, Yeh D-M, Huang C-F, Huang J-J and Yang C-C 2006 Orange–red light-emitting diodes based on a prestrained InGaN–GaN quantum-well epitaxy structure *IEEE Photon. Technol. Lett.* **18** 2269–71

[213] Shon J W, Ohta J, Ueno K, Kobayashi A and Fujioka H 2014 Fabrication of full-color InGaN-based light-emitting diodes on amorphous substrates by pulsed sputtering *Sci. Rep.* **4** 5325

[214] Li P, Li H, Li Z, Kang J, Yi X, Li J and Wang G 2015 Strong carrier localization effect in carrier dynamics of 585 nm InGaN amber light-emitting diodes *J. Appl. Phys.* **117** 073101

[215] Lee K, Choi I, Lee C-R, Chung T-H, Kim Y S, Jeong K-U, Chung D C and Kim J S 2017 Flower-like internal emission distribution of LEDs with monolithic integration of InGaN-based quantum wells emitting narrow blue, green, and red spectra *Sci. Rep.* **7** 7164

[216] Lee K, Lee H, Lee C-R, Chung T-H, Kim Y S, Leem J-Y, Jeong K-U and Kim J S 2017 Yellow-red light-emitting diodes using periodic Ga-flow interruption during deposition of InGaN well *Opt. Express* **25** 15152–60

[217] Zhuang Z, Iida D, Velazquez-Rizo M and Ohkawa K 2021 606-nm InGaN amber micro-light-emitting diodes with an on-wafer external quantum efficiency of 0.56% *IEEE Electron Device Lett.* **42** 1029–32

[218] Li H, Cheng H-Y, Chen W-L, Huang Y-H, Li C-K, Chang C-Y, Wu Y-R, Lu T-C and Chang Y-M 2017 Three

dimensional characterization of GaN-based light emitting diode grown on patterned sapphire substrate by confocal Raman and photoluminescence spectromicroscopy *Sci. Rep.* **7** 45519
[219] Keller S *et al* 2014 Recent progress in metal-organic chemical vapor deposition of (000–1) N-polar group-III nitrides *Semicond. Sci. Technol.* **29** 113001
[220] Mizokami Y, Werner J S, Crognale M A and Webster M A 2006 Nonlinearities in color coding: compensating color appearance for the eye's spectral sensitivity *J. Vis.* **6** 996–1007
[221] Damilano B and Gil B 2015 Yellow–red emission from (Ga,In)N heterostructures *J. Phys. D: Appl. Phys.* **48** 403001
[222] Xu T, Nikiforov A Y, France R, Thomidis C, Williams A and Moustakas T D 2007 Blue-green-red LEDs based on InGaN quantum dots grown by plasma-assisted molecular beam epitaxy *Phys. Status Solidi* a **204** 2098–102
[223] Soh C B, Liu W, Chua S J, Ang S S, Tan R J N and Chow S Y 2010 Generation of amber III-nitride based light emitting diodes by indium rich InGaN quantum dots with InGaN wetting layer and AlN encapsulation layer *J. Appl. Phys.* **108** 093501
[224] Nguyen H P T, Zhang S, Cui K, Korinek A, Botton G A and Mi Z 2012 High-efficiency InGaN/GaN dot-in-a-wire red light-emitting diodes *IEEE Photon. Technol. Lett.* **24** 321–3
[225] Kishino K, Nagashima K and Yamano K 2013 Monolithic integration of InGaN-based nanocolumn light-emitting diodes with different emission colors *Appl. Phys. Express* **6** 012101
[226] Kishino K, Yanagihara A, Ikeda K and Yamano K 2015 Monolithic integration of four-colour InGaN-based nanocolumn LEDs *Electron. Lett.* **51** 852–4
[227] Philip M R, Choudhary D D, Djavid M, Le K Q, Piao J and Nguyen H P T 2017 High efficiency green/yellow and red InGaN/AlGaN nanowire light-emitting diodes grown by molecular beam epitaxy *J. Sci.: Adv. Mater. Devices* **2** 150–5
[228] Meyaard D S, Shan Q, Cho J, Fred Schubert E, Han S-H, Kim M-H, Sone C, Jae O S and Kyu Kim J 2012 Temperature dependent efficiency droop in GaInN light-emitting diodes with different current densities *Appl. Phys. Lett.* **100** 081106
[229] Chhajed S, Xi Y, Li Y L, Gessmann T and Schubert E F 2005 Influence of junction temperature on chromaticity and color-rendering properties of trichromatic white-light sources based on light-emitting diodes *J. Appl. Phys.* **97** 054506
[230] Iida D, Lu S, Hirahara S, Niwa K, Kamiyama S and Ohkawa K 2016 Investigation of amber light-emitting diodes based on InGaN/AlN/AlGaN quantum wells *Jpn. J. Appl. Phys.* **55** 05FJ06
[231] Zhuang Z, Iida D and Ohkawa K 2020 Effects of size on the electrical and optical properties of InGaN-based red light-emitting diodes *Appl. Phys. Lett.* **116** 173501
[232] Lee H K, Lee D H, Song Y M, Lee Y T and Yu J S 2011 Thermal measurements and analysis of AlGaInP/GaInP MQW red LEDs with different chip sizes and substrate thicknesses *Solid·State Electron.* **56** 79–84
[233] Kim M S, Lee H K and Yu J S 2013 Device characteristics and thermal analysis of AlGaInP-based red monolithic light-emitting diode arrays *Semicond. Sci. Technol.* **28** 025005
[234] Mukai T, Yamada M and Nakamura S 1998 Current and temperature dependences of electroluminescence of InGaN-based UV/blue/green light-emitting diodes *Jpn. J. Appl. Phys.* **37** L1358–61